9

Synthesis of the Seismic Structure of the Greater Alaska Region: Geodynamics Implications

Margarete A. Jadamec[1,2], Gary L. Pavlis[3], Xiaotao Yang[4], Karen M. Fischer[5], Songqiao Shawn Wei[6], Michael Everett Mann[5], and Andrew John Schaeffer[7]

ABSTRACT

EarthScope has fundamentally improved the characterization of the crust and mantle structure within and below the North American plate in Alaska and northwestern Canada. This study reviews the geodynamic implications of recent EarthScope seismic synthesis results in the context of recent and classic geodynamic models of both location-specific and generalized subduction, and the limitations of models therein. In particular, the study examines constraints geodynamic models place on the tectonic implications of the improved upper plate, slab, and mantle structure for slab dynamics, mantle flow, and upper plate deformation. First-order remaining questions are identified for the Aleutian–Alaska subduction zone, interior Alaska, and northwestern Canada, including how deeper slab structure may affect trench motion and upper plate deformation, mechanisms of flat slab subduction, and the role of the Yakutat plateau subduction-collision in these processes. EarthScope seismic syntheses for Alaska are considered in the larger context of the Pacific Ring of Fire multi-plate system, of which the Aleutian–Alaska subduction zone forms the northern boundary. Similarities and differences with other subduction zones along the Pacific Ring of Fire are examined, with the Aleutian–Alaska subduction zone serving as a window to tectonic processes elsewhere along the Pacific Ring of Fire.

9.1. INTRODUCTION

9.1.1. Background and Motivation

Over a decade's worth of EarthScope data have provided new constraints on the seismic and tectonic structure of the central and northwestern North American Plate, as well as the underlying mantle and subducted slabs (Burdick et al., 2008, 2017; Miller et al., 2020; Williams et al., 2010). Through an integrated and systematic footprint of seismic and geodetic instruments, the EarthScope data collection efforts spatially and temporally swept across the contiguous United States moving from the active tectonic boundary along the west coast toward the passive continental margin on the east

[1]*Department of Geology, University at Buffalo, Buffalo, NY, USA*
[2]*Institute for Artificial Intelligence and Data Science, University at Buffalo, Buffalo, NY, USA*
[3]*Department of Earth and Atmospheric Sciences, Indiana University Bloomington, Bloomington, IN, USA*
[4]*Department of Earth, Atmospheric, and Planetary Sciences, Purdue University, West Lafayette, IN, USA*
[5]*Department of Earth, Environmental, and Planetary Sciences, Brown University, Providence, RI, USA*
[6]*Department of Earth and Environmental Sciences, Michigan State University, East Lansing, MI, USA*
[7]*Geological Survey of Canada, Natural Resources Canada, Sidney, Canada*

Tectonics and Seismic Structure of Alaska and Northwestern Canada: EarthScope and Beyond, Geophysical Monograph 290, First Edition.
Edited by Natalia A. Ruppert, Margarete A. Jadamec, and Jeffrey T. Freymueller.

DOI: 10.1002/9781394195947.ch9
Companion website: www.wiley.com/go/Ruppert

coast, and lastly moving northwestward up to Alaska and northwestern Canada (Burdick et al., 2008, 2017; Miller et al., 2020; Williams et al., 2010).

This study is one of three chapters from the same group that synthesize the EarthScope seismic studies in Alaska and northwestern Canada. This chapter focuses on the geodynamic implications of the recent seismic synthesis efforts for the crust and mantle structure in Alaska and northwestern Canada (Yang et al., 2024) and the slab and mantle structure beneath Alaska and northwestern Canada (Pavlis et al., 2024). This chapter frames the seismic synthesis results (Pavlis et al., 2024; Yang et al., 2024) in a large-scale three-dimensional (3-D) tectonic framework and examines the interrelation between the lithospheric plates, asthenosphere, and transition zone for the greater Alaska region through the lens of geodynamics. We discuss the implications of new constraints on the 3-D distribution of the major crustal and lithospheric domains, lithospheric discontinuities, and depth constraints on the lithosphere–asthenosphere boundary and how these relate to the slab structure including the morphology of the flat slab region and slab terminus in eastern Alaska, the slab geometry at depth, as well as subducted oceanic fragments now immersed in the asthenosphere. A brief review of continuum models of subduction is provided, with emphasis on the insights gained from generalized as well as geographically referenced models as they relate to subduction dynamics in the Aleutian–Alaska system. To further expand the framework, the synthesis is presented in the context of observational constraints on the larger Pacific Ring of Fire tectonic system, of which the Aleutian–Alaska subduction zone forms the northern boundary (Figures 9.1 and 9.2) (DeMets et al., 1994; Hayes et al., 2018; Jadamec et al., 2018b; Müller et al., 2019; Seton et al., 2020; Smithsonian, 2012; Tozer et al., 2019).

9.1.2. Context of the Aleutian–Alaska Subduction Zone within the Pacific Ring of Fire Multiplate System

The Pacific Ring of Fire is a tectono-physiographic term for the collection of subduction zones that outwardly flank the eastern, northern, and western perimeters of the Pacific Ocean, forming a horseshoe-shaped region of tectonic activity that opens to the south (Figures 9.1b and 9.2b) (DeMets et al., 1994; Hayes et al., 2018; Jadamec et al., 2018b; Müller et al., 2019; Seton et al., 2020; Smithsonian et al., 2012; Tozer et al., 2019). The oceanic plates subducting along the Pacific Ring of Fire include, by decreasing size, the Pacific Plate, Nazca Plate, Philippine Plate, Cocos Plate, Juan de Fuca Plate, Rivera Plate, and additional microplates in the southwest Pacific (Figures 9.1 and 9.2) (Argus et al., 2011; Bird, 2003; DeMets et al., 2010, 1994; Hayes et al., 2018; Jadamec et al., 2018b; Müller et al., 2019; Seton et al., 2020; Tozer et al., 2019). Thus, overall there is a collective system of subducting oceanic plates comprising the Pacific Ring of Fire, of which the Pacific Plate is the largest (Schellart et al., 2008; Argus et al., 2011; Bird, 2003; DeMets et al., 2010, 1994; Müller et al., 2019; Seton et al., 2020).

The northern limit of the Pacific Ring of Fire is bounded by the Aleutian–Alaska subduction zone (Section 9.1.3) (Argus et al., 2011; Bird, 2003; DeMets et al., 2010, 1994; Plafker, Mooreand & Winkler, 1994; Seton et al., 2020; Tozer et al., 2019). The western flank of the Pacific Ring of Fire can be described as a zone rather than being defined by a single trench (Figures 9.1b and 9.2b). In the northwestern region, the Pacific Plate subducts northwestward along the Kamchatka–Kuril–Japan trench (Figures 9.1b and 9.2b) (DeMets et al., 1994; Hayes et al., 2018; Jadamec et al., 2018b; Müller et al., 2019; Seton et al., 2020; Tozer et al., 2019). The Kamchatka–Kuril–Japan trench continues south into the Izu–Bonin–Mariana trench, where the Pacific Plate subducts northwestward beneath the Philippine Sea Plate (Figures 9.1b and 9.2b) (Argus et al., 2011; Bird, 2003; DeMets et al., 2010, 1994; Hayes et al., 2018; Jadamec et al., 2018b; Müller et al., 2019; Seton et al., 2020; Tozer et al., 2019). Farther to the west, the oceanic Philippine Sea Plate is in turn subducting northwestward along the Ryukyu–Nankai trench, as well as along the Philippines trench to the southwest, with additional complicated configurations along the Manila trench and near the southern tip of the Philippine Plate (Figures 9.1b and 9.2b) (Argus et al., 2011; Bird, 2003; DeMets et al., 2010, 1994; Hayes et al., 2018; Jadamec et al., 2018b; Müller et al., 2019; Seton et al., 2020; Tozer et al., 2019). The southwestern Pacific Ring of Fire also contains both large and small subduction zones (Figures 9.1b and 9.2b). This includes subduction zones dipping both north and south in the broader Solomon Islands region, the larger northeast dipping slab at the New Hebrides trench, and the even larger westward dipping slab along the Tonga–Kermadec–Hikurangi trench (Figures 9.1b and 9.2b) (Argus et al., 2011; Bird, 2003; DeMets et al., 2010, 1994; Hayes et al., 2018; Jadamec et al., 2018b; Müller et al., 2019; Seton et al., 2020; Tozer et al., 2019). Note that in the New Hebrides subduction zone, the Pacific Plate and associated microplates of the North Fiji basin are the upper plate, whereas in the Tonga–Kermadec–Hikurangi subduction zone, the Pacific Plate is the downgoing plate (Figures 9.1b and 9.2b) (Argus et al., 2011; Bird, 2003; DeMets et al., 2010, 1994; Hayes et al., 2018; Jadamec et al., 2018b; Müller et al., 2019; Seton et al., 2020; Tozer et al., 2019).

Subduction on the eastern side of the Pacific Ring of Fire is defined by the Cascadia, Middle America, and Columbia-Peru-Bolivia-Chile trenches (Figures 9.1b

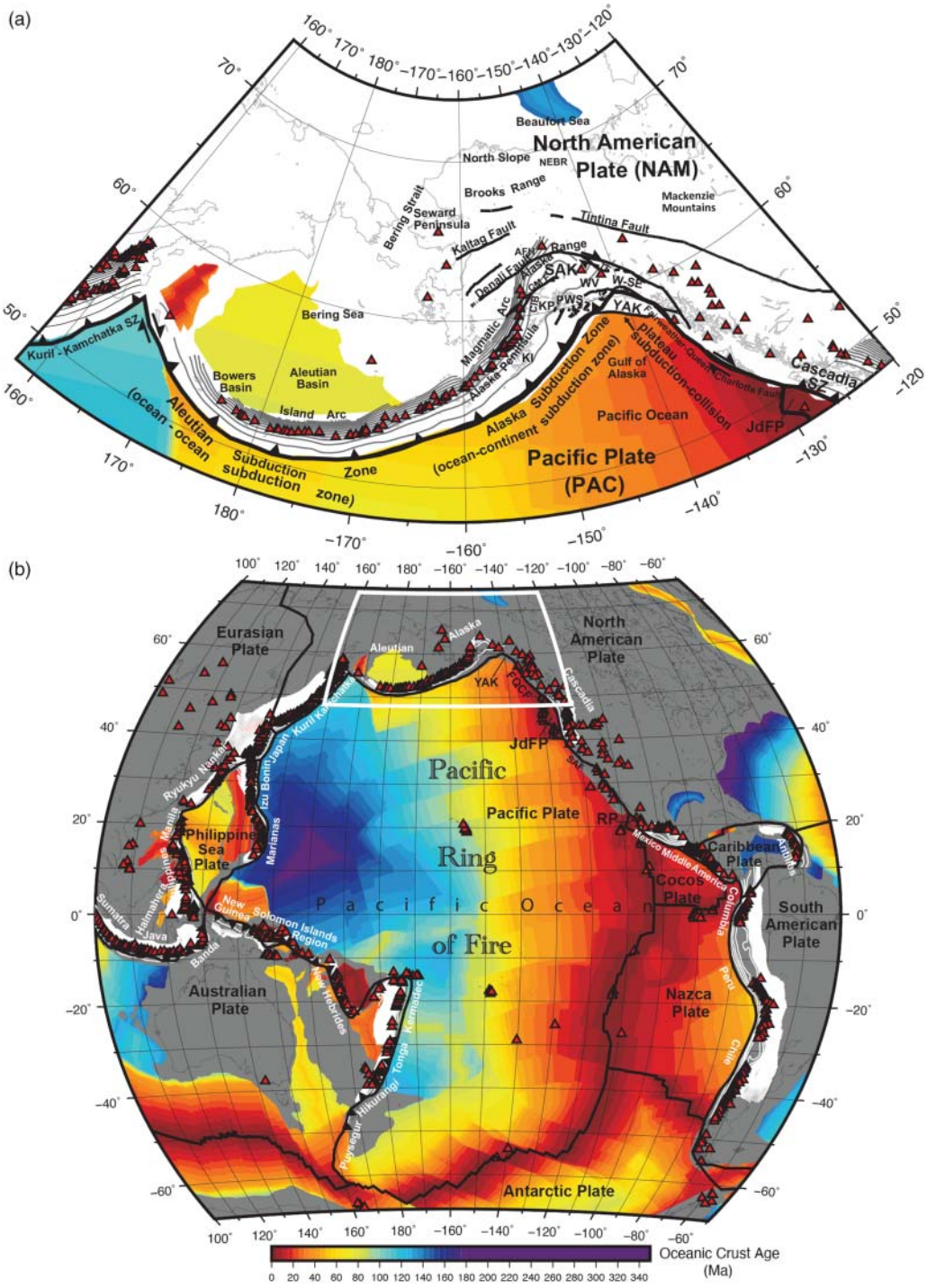

Figure 9.1 Tectonic setting of (a) the Aleutian–Alaska subduction zone in (b) larger tectonic context of the Pacific Ring of Fire. The white box in (b) outlines the location of (a). Basemap: age of oceanic crust (Müller et al., 2019; Seton et al., 2020). Thick black lines: major plate boundaries (DeMets et al., 1994). Thin black lines: Faults (Plafker, Gilpin, & Lahr, 1994). Thin dark gray lines (a) and thin white lines (b): depth contours of the slab surface in 20 km intervals (Hayes et al., 2018). Triangles: Holocene volcanoes (Smithsonian, 2012). Major subduction zone names in white labels. (a) Labels: AKF, Alaska Range Foothills; CIB, Cook Inlet Basin; CMF, Castle Mountain Fault; KI, Kodiak Island; KP, Kenai Peninsula; NEBR, Northeastern Brooks Range; PWS, Prince William Sound; TF, Totschunda Fault; YAK, Yakutat plateau; WR, Wrangell volcanics; W-SE, Wrangell–St. Elias Mountains. (b) Labels: FWQC, Fairweather-Queen Charlotte Fault; JdFP, Juan de Fuca Plate; RP, Rivera Plate; YAK, Yakutat plateau. Map was made with GMT (Wessel et al., 2013).

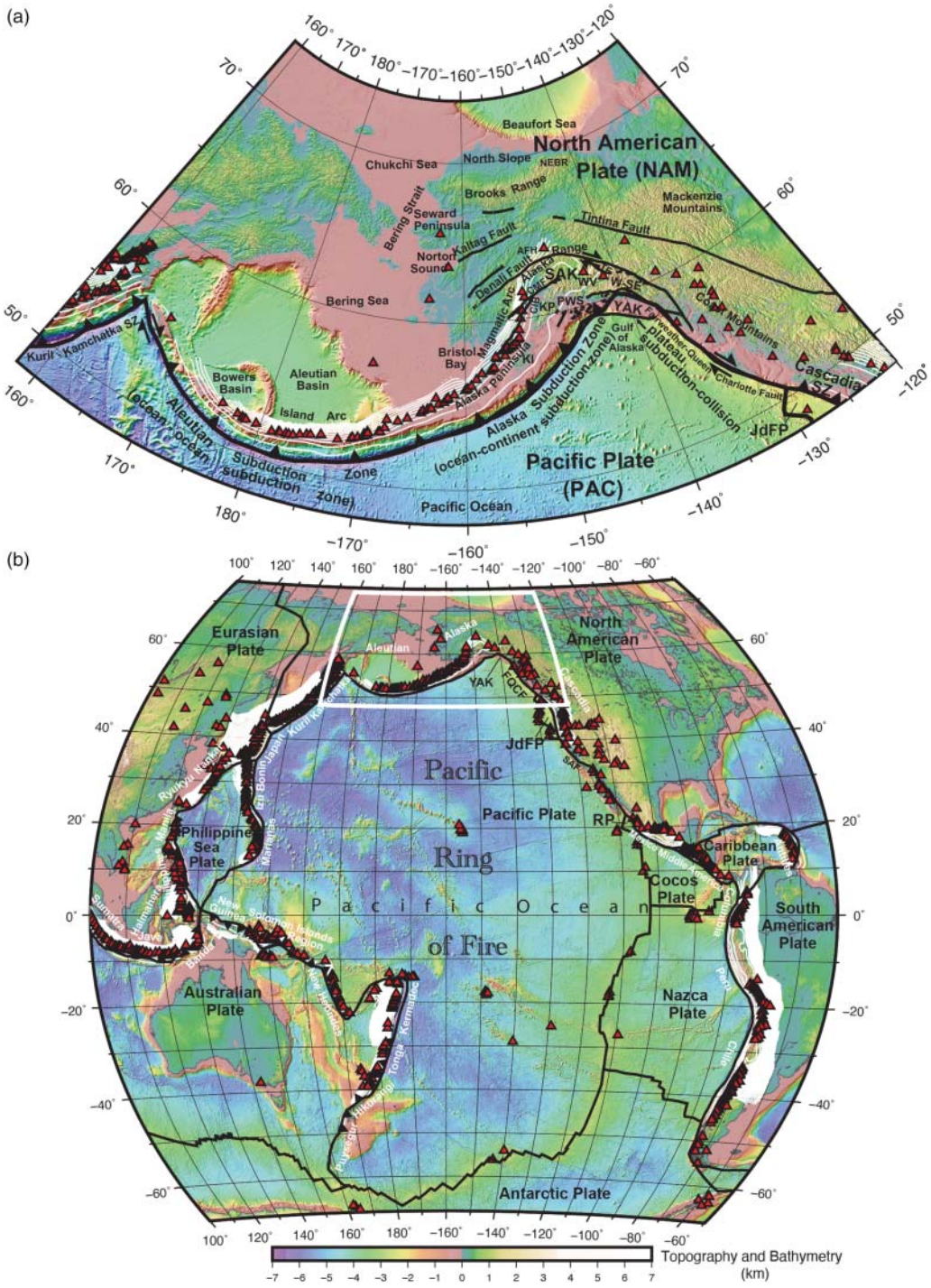

Figure 9.2 Tectonic setting of (a) the Aleutian–Alaska subduction zone in (b) larger tectonic context of the Pacific Ring of Fire. The white box in (b) outlines the location of (a). Basemap: bathymetry and topography from Tozer et al. (2019). Thin white lines: depth contours of the slab surface in 20 km intervals (Hayes et al., 2018). All other data are same as in Figure 9.1.

and 9.2b) (Argus et al., 2011; Bird, 2003; Schellart et al., 2008; DeMets et al., 2010, 1994; Hayes et al., 2018; Jadamec et al., 2018b; Müller et al., 2019; Seton et al., 2020; Tozer et al., 2019). In addition, the Antilles and Scotia subduction zones are located outboard to the east, and although not geographically flanking the Pacific Ocean, both have associations with the larger Pacific Ring of Fire plate tectonic system through smaller plates partially bounded on the north and south by strike-slip boundaries (Figures 9.1b and 9.2b) (Argus et al., 2011; Bird, 2003; DeMets et al., 2010, 1994; Hayes et al., 2018; Jadamec et al., 2018b; Müller et al., 2019; Seton et al., 2020; Tozer et al., 2019).

9.1.3. Tectonic Setting of the Aleutian–Alaska Subduction Zone

The Aleutian–Alaska subduction zone forms the northern boundary of the Pacific Ring of Fire (Figures 9.1 and 9.2) (DeMets et al., 1994; Plafker, Moore, & Winkler, 1994; Seton et al., 2020; Tozer et al., 2019). Here, along the Aleutian–Alaska trench, the massive oceanic Pacific Plate (DeMets et al., 1994; Müller et al., 2019; Seton et al., 2020) subducts northwestward (DeMets et al., 1994; Hayes et al., 2018; Plafker, Moore, & Winkler, 1994; Tozer et al., 2019), causing large-scale deformation of the North American Plate in Alaska and northwestern Canada (Elliott & Freymueller, 2020; Jadamec et al., 2013; Plafker & Berg, 1994) and inducing 3-D mantle flow in the underlying asthenosphere (Billen & Gurnis, 2003; Jadamec & Billen, 2010, 2012). The western terminus of the Aleutian–Alaska subduction zone is defined by a corner-shaped intersection with the northeast-trending Kuril–Kamchatka subduction zone, forming the northwestern corner of the Pacific Ring of Fire (Figure 9.1 and 9.2) (DeMets et al., 1994; Plafker, Moore, & Winkler, 1994; Seton et al., 2020; Tozer et al., 2019). The eastern terminus of the Aleutian–Alaska subduction zone is also defined by a corner-shaped zone of tectonic complexity, transitioning from plateau subduction-collision eastward into the Fairweather-Queen Charlotte transform system (Eberhart-Phillips et al., 2006; Pavlis et al., 2019). This complex zone demarcates the northeastern corner of the Pacific Ring of Fire (Figures 9.1 and 9.2).

Following the NUVEL-1A tectonic plate configurations (DeMets et al., 1994), the upper plate of the Aleutian–Alaska subduction zone is the North American Plate (Figures 9.1a and 9.2a). In the western portion of the Aleutian–Alaska subduction zone, the overriding plate is comprised of oceanic lithosphere in the Aleutian Basin, making the western half of the Aleutian–Alaska subduction zone an ocean–ocean subduction zone at the trench (Figures 9.1a and 9.2a) (Müller et al., 2019; Seton et al., 2020). This ocean–ocean portion of the subduction zone is hereafter referred to as the Aleutian segment (Figures 9.1a and 9.2a). In the eastern portion of the subduction zone, the overriding plate is comprised of a series of amalgamated terranes that were transported to the present location in the Mesozoic to Cenozoic, as well as inboard North American continental material, making the eastern half of the Aleutian–Alaska subduction zone an ocean–continent subduction zone (Colpron et al., 2007; Fuis et al., 1991; Moore & Box, 2016; Nokleberg, MollStalcup, et al., 1994; Nokleberg, Plafker, & Wilson, 1994; Plafker, Gilpin, & Lahr, 1994; Torne et al., 2019). This ocean–continent portion of the subduction zone is hereafter referred to as the Alaska segment (Figures 9.1a and 9.2a) and is characterized by large-scale active faulting (Eberhart-Phillips et al., 2003; Fisher et al., 2004; Koehler et al., 2018; Ratchkovski et al., 2004) and deformation (Benowitz et al., 2011; C. A. Burkett et al., 2016; Elliott & Freymueller, 2020; Plafker & Berg, 1994; Ratchkovski & Hansen, 2002a).

The curvature of the Aleutian–Alaska trench varies along its length in both facing direction and radius (Bird, 2003; DeMets et al., 1994; Tozer et al., 2019). The trench defines a broad concave-to-the-north arc in the west that changes into a convex-to-the-north arc with a smaller radius of curvature in the east (Figures 9.1a and 9.2a). Synthesized estimates of trench motion (Schellart et al., 2008) indicate a change in trench-perpendicular retreat rate along the length of the Aleutian–Alaska trench. From west to east, the values decrease from 1.9, to 1.2, to 0.6 cm/yr in the modified Indo-Atlantic hot spot reference frame and from 2.4, to 2.2, to 1.7 cm/yr in the No-net rotation reference frame (Schellart et al., 2008). Alternatively, in the Pacific hot spot reference frame, synthesized trench motion estimates indicate trench-perpendicular advance, with rates changing from 0.1, to 0.5, to 0.2 cm/yr from west to east along the Aleutian–Alaska trench (Schellart et al., 2008). Thus, there is less trench-perpendicular retreat in the Alaska segment versus the Aleutian segment, or greater trench perpendicular advance in the Alaska segment than in the Aleutian segment of the subduction zone, depending on the reference frame.

The large-scale structure of the subducting plate geometry in the Aleutian–Alaska subduction zone is characterized by a curved slab that is concave to the north and dips moderately to steeply in the Aleutian segment of the subduction zone and a moderate to shallowly dipping curved slab that is convex to the north in the Alaska segment (Figures 9.1a and 9.2a) (Gudmundsson & Sambridge, 1998; Hayes et al., 2018; Jadamec et al., 2018b; Syracuse & Abers, 2006; Zhao et al., 1995). The geometry of the slab is less well resolved at the lateral terminations of the subduction zone. For example, in the western terminus, although the Slab2.0 slab geometry

model demarcates the Kuril–Kamchatka slab extending northward up to the intersection of the Kuril–Kamchatka trench with the Aleutian–Alaska trench, the Aleutian slab segment is discontinuous as it approaches this intersection, with the discontinuities spanning ~8° longitude eastward from this intersection (Figures 9.1a and 9.2a). In the eastern terminus of the Aleutian–Alaska subduction zone, the slab becomes flat beneath Alaska with an arched tabletop-like structure (Fuis et al., 2008; Gou et al., 2019; Jadamec & Billen, 2016b; Jadamec et al., 2018b; Mann et al., 2022; Nayak et al., 2020; Ratchkovski & Hansen, 2002b; Veilleux & Doser, 2007; Yang & Gao et al., 2020; Zhao et al., 1995). However, here the geometry becomes complicated, with varying depth extents of the slab and regions of segmentation and scales of discontinuities (Fuis et al., 2008; Gou et al., 2019; Jadamec & Billen, 2016b; Jadamec et al., 2018b; Mann et al., 2022; Nayak et al., 2020; Ratchkovski & Hansen, 2002b; Veilleux & Doser 2007; Yang & Gao 2020).

The age of the incoming Pacific Plate varies along the length of the Aleutian–Alaska trench (Müller et al., 2019; Seton et al., 2020), decreasing from ~120 Ma in the west to ~25 Ma in the east (Figure 9.1). The gradients in seafloor age of the Pacific Plate are variable along the length of the trench reflecting variations in paleoplate motions (Müller et al., 2019; Sdrolias & Müller, 2006; Seton et al., 2020). The bathymetry beneath the northern Pacific Ocean shows a west to east decrease in water depth that correlates with the eastward younging in seafloor age (Figures 9.1 and 9.2) (Bird, 2003; Müller et al., 2019; Seton et al., 2020; Tozer et al., 2019). The northwestern Pacific Plate contains seamounts, related to the Hawaiian hot spot track, intersecting with the Aleutian–Alaska subduction zone near the corner-shaped juncture with the Kuril–Kamchatka trench (Figure 9.2). In the eastern corner of the subduction zone, the unsubducted portion of the subducting-colliding Yakutat microplate has a bathymetric elevation comparable to that of the nearby continental shelf (Figure 9.2) (Bird, 2003; Müller et al., 2019; Seton et al., 2020; Tozer et al., 2019). Seismic studies indicate Yakutat crust has an eastward thickening wedge shape, of 11 km at its western end and reaches over 30 km at its eastern end (Christeson et al., 2010; Fuis et al., 2008; Kim et al., 2014; Mann et al., 2022; Pavlis et al., 2019; Rondenay et al., 2010; Rossi et al., 2006; Worthington et al., 2012).

Holocene volcanism along the Aleutian island arc-Alaska magmatic arc (Smithsonian, 2012) is relatively continuous (Figures 9.1a and 9.2a). However, there are notable volcanic gaps along the length of the Aleutian–Alaska subduction zone (Smithsonian, 2012). In the westernmost portion of the subduction zone, there is a volcanic gap that extends west of Bowers Basin to just before the intersection with the Kuril–Kamchatka subduction zone (Figures 9.1a and 9.2a). The Aleutian-Alaska volcanic arc has a volcanic gap in south-central Alaska, which is spatially coincident with the flat slab section of the subduction zone (Figures 9.1a and 9.2a) (Hayes et al., 2018; Millet et al., 2023; Rabade et al., 2023; Rondenay et al., 2010; Smithsonian, 2012). This volcanic gap is bordered to the east by a cluster of volcanoes associated with the Wrangell volcanic field (Brueseke et al., 2023, 2019; Preece & Hart, 2004; Skulski et al., 1991), which may be related to discontinuities in the slab (Fuis et al., 2008; Jadamec & Billen, 2010, 2012; Pavlis et al., 2019) and related slab-edge-driven mantle flow dynamics (Jadamec & Billen, 2010, 2012; Jadamec et al., 2012; Jadamec, 2016a). In addition, there are Holocene volcanoes farther inboard, in western Alaska and southeast Alaska (Smithsonian, 2012), which have a genetic origin that is less well known (Figures 9.1a and 9.2a).

9.2. EARTHSCOPE SEISMIC SYNTHESES

Seismic studies and syntheses of EarthScope data for Alaska and northwestern Canada are presented in detail in multiple chapters throughout this volume. This section summarizes how the results of two companion EarthScope seismic synthesis studies (Pavlis et al., 2024; Yang et al., 2024) provide new insights on the geodynamics of the Aleutian–Alaska system, with large-scale implications for other subduction zones in the Pacific Ring of Fire discussed in the Discussion section.

9.2.1. Crust and Lithosphere Structure Synthesis Study

Within continental Alaska, there are a series of amalgamated tectonic terranes and large-scale faults (Figure 9.3a) (Colpron et al., 2007; Fuis et al., 1991; Koehler et al., 2018; Moore & Box, 2016; Nokleberg, Plafker, & Wilson, 1994; Plafker, Gilpin, & Lahr, 1994). Major fault systems include the Kobuk Fault Zone along the southern border of the Brooks Range in northern Alaska, the Kaltag and Tintina faults in central Alaska, and the Denali Fault System in southcentral Alaska (Plafker, Gilpin, & Lahr, 1994). To examine the relationship between crustal and mantle seismic structures and major faults and tectonic terranes, as one of the two companion chapters, Yang et al. (2024) analyzed eight 3-D shear-wave velocity models (Berg et al., 2020; Feng & Ritzwoller, 2019; Gama et al., 2022b; Jiang et al., 2018; Martin-Short et al., 2018; Nayak et al., 2020; Ward & Lin, 2018; Yang & Gao, 2020) and seven crustal thickness models (Gama et al., 2022a; Haney et al., 2020; Mann et al., 2022; Miller & Moresi, 2018; Rossi et al., 2006;

Veenstra et al., 2006; Zhang et al., 2019). To compare the 3-D shear-wave velocity models objectively, Yang et al. (2024) used an unsupervised K-means clustering of 1-D velocity profiles, constructed from the 3-D models resampled onto a common grid and smoothed. The resultant vote maps of cluster boundaries (Figure 9.3b-c) highlight velocity domain boundaries that are consistent across multiple velocity models (Yang et al., 2024). In addition, Yang et al. (2024) calculated average crustal thicknesses from the seven published models.

The regionalization of the 3-D velocity models from Yang et al. (2024) allows for spatial similarities in seismic properties of the crust and mantle to be identified objectively without considering terrane locations a priori. Most of the seismic velocity domain boundaries strike approximately parallel to the trends of the tectonic terranes and major faults in Alaska (Figure 9.3d). In southern Alaska, some of these trends are approximately east–west but concave to the south, parallel to the active convergent margin (e.g., domains C6 and M5). In northern Alaska, some structural trends are concave to the north (e.g., C1–C3), reflecting more ancient accretionary tectonic terranes. The velocity model clustering and crustal thickness analyses indicate that the Denali Fault System, the Kobuk Fault Zone, and potentially the Porcupine Shear Zone represent lithospheric-scale boundaries that separate regions with distinct seismic structures (Figure 9.3e). The relationships of the Kaltag and Tintina faults to crustal and mantle domains are more complex. The seismic velocity domains and the crustal thickness patterns shed light on the direction of future seismic, tectonic, and geodynamical studies.

9.2.2. Slab and Mantle Structure Synthesis Study

In the second of the three EarthScope seismic synthesis companion chapters, Pavlis et al. (2024) examined four teleseismic body-wave models (Burdick et al., 2017; Estève et al., 2020; Esteve et al., 2019; Gou et al., 2019; Jiang et al., 2018) and two receiver function imaging studies (Bauer et al., 2014; Mann et al., 2022). For the body-wave models, perturbations in P velocity (Burdick et al., 2017; Esteve et al., 2019; Estève et al., 2020; Gou et al., 2019) and S velocity (Esteve et al., 2019; Estève et al., 2020; Jiang et al., 2018) were examined. The receiver function imaging studies examined perturbations in P and S velocities (Mann et al., 2022) as well as S–P amplitude (Bauer et al., 2014). The synthesis results were then compared in Pavlis et al. (2024) qualitatively using graphical comparisons and quantitatively using vote maps. The voting metric used in Pavlis et al. (2024) followed the approach in Shephard et al. (2017) but with normalized votes due to the variable coverage in the regional studies of Alaska with analysis to depths of approximately 800 km. The vote maps were used to assess commonalities between the models in the location of positive velocity anomalies, that is velocities faster than the background (Pavlis et al., 2024). More details on the method and threshold specificity are given in Pavlis et al. (2024). Key features from that chapter important for this one are illustrated in Figure 9.4.

9.2.3. Key Findings of EarthScope Seismic Syntheses

Our two companion chapters contain the following observations important for geodynamics in Alaska:

1. There is now strong evidence that the eastern edge of the subduction zone downstream from the Yakutat microplate is associated with a lateral tear. The current models are convergent in showing that the tear section begins southwest of the Wrangells and terminates at a depth between 300 and 400 km.
2. Below the flat slab region, the slab appears to be folded to the south forming a lithospheric scale recumbent fold with the nose of the fold under the northern limit of the slab known previously from seismicity. That geometry was not known prior to EarthScope.
3. The near-vertical section of the flat slab fold may extend eastward to form a vertical sheet from the base of Alaskan lithosphere to the top of the transition zone. That structure is terminated to the east very close to the edge predicted from plate kinematics by Pavlis et al. (2019). In our companion chapter (Pavlis et al., 2024), we hypothesize that this EarthScope discovery, which we called the Yukon River anomaly, marks the grave of the slab subducted prior to the tear downstream from the current location of the Yakutat microplate.
4. There is now unambiguous evidence for a high-velocity body under the Yukon. It has a distinct separation above the transition zone from the Yakutat tear fragment and the Yukon River anomaly. Fuston and Wu (2020) call this anomaly the "Yukon slab" and argue that it can be explained as a remnant of late Mesozoic and early Cenozoic subduction of the Kula Plate prior to the major change in Pacific Plate motion around 40 Ma.
5. Although the models are not as convergent, the tomography models indicate the slab descends through the transition zone with a southward dip under parts of southern Alaska. Differences among the models are likely linked to the relative velocity anomalies being weaker in the transition zone and/or resolution limitations of the existing models. The models are more convergent in showing a high-velocity anomaly below the transition zone southeast of the modern trench under the Gulf

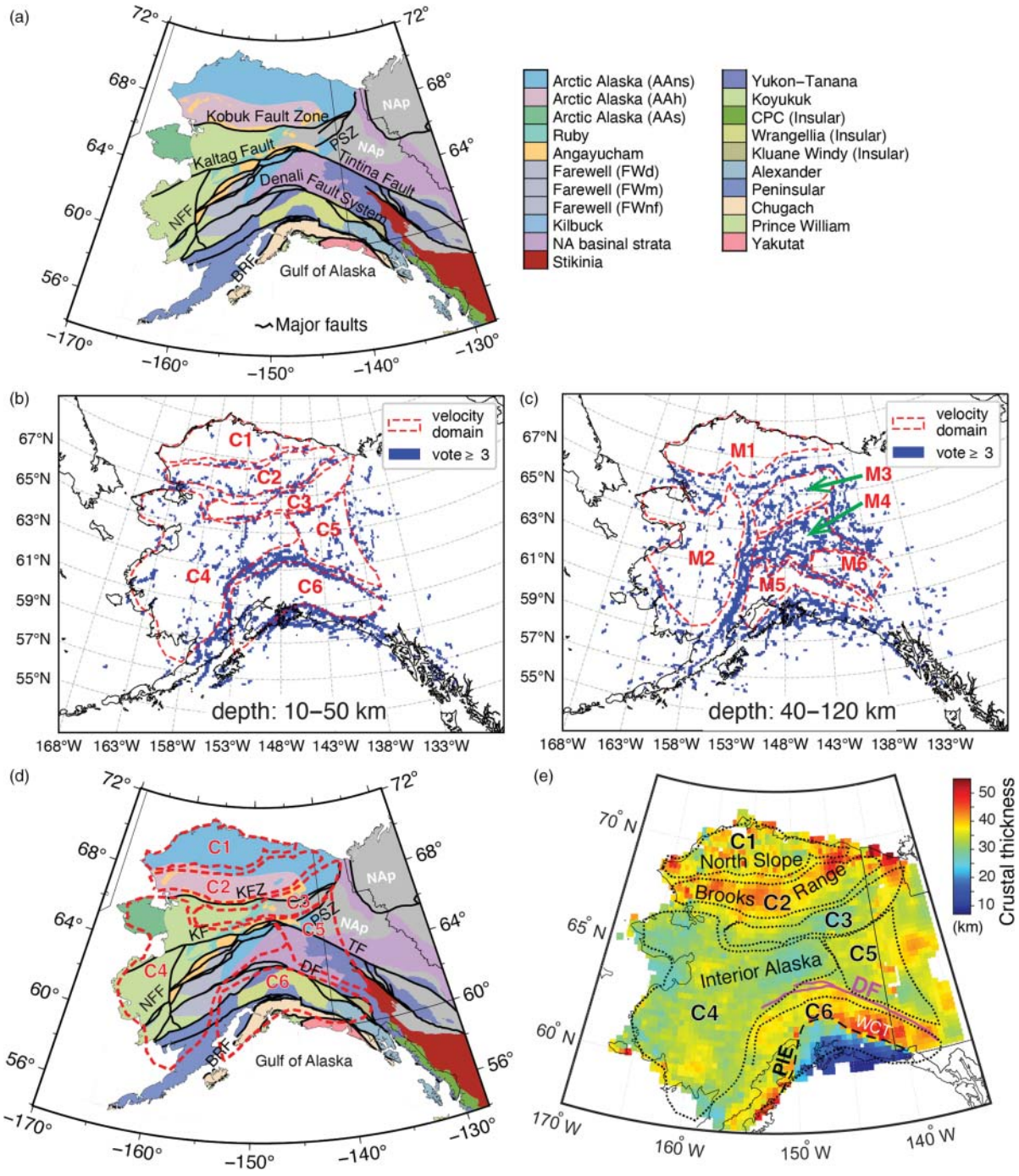

Figure 9.3 Major seismic structural domains of the continental lithosphere from syntheses of seismic velocity and crustal thickness models Yang et al. (Accepted, 2023)/Xiaotao Yang. (a) Major tectonic terranes comprising mainland Alaska based on Colpron et al. (2007). Fault labels: PSZ, Porcupine Shear Zone; NFF, Nixon Fork-Iditarod Fault; BRF, Border Range Fault. Terrane labels: AAns, Arctic Alaska North Slope subterrane; AAh, Arctic Alaska Hammond-Coldfoot subterrane; AAs, Arctic Alaska Seward subterrane; FWd, Farewell Dillinger subterrane; FWm, Farewell Mystic subterrane; FWnf, Farewell Nixon Fork subterrane; CPC, Coast Plutonic Complex; NAp, North America platformal strata in western Laurentia. (b,c) Major crustal, C1–C6 in (b) and upper mantle, M1–M6 in (c), seismic velocity domains from clustering analysis. The blue background shows the cluster boundaries shared by at least three velocity models. (d,e) Comparisons of crustal velocity domains (C1–C6) with (d) tectonic terranes and (e) average crustal thickness patterns. The crustal thickness model is from Yang et al. (Accepted, 2023)/Xiaotao Yang. DF, Denali Fault; WCT, Wrangell Composite Terrane; PIE, Plate Interface Extent [defined in Yang et al. (Accepted, 2023)/Xiaotao Yang]. Panels (a), (d), and (e) are made with GMT (Wessel et al., 2013).

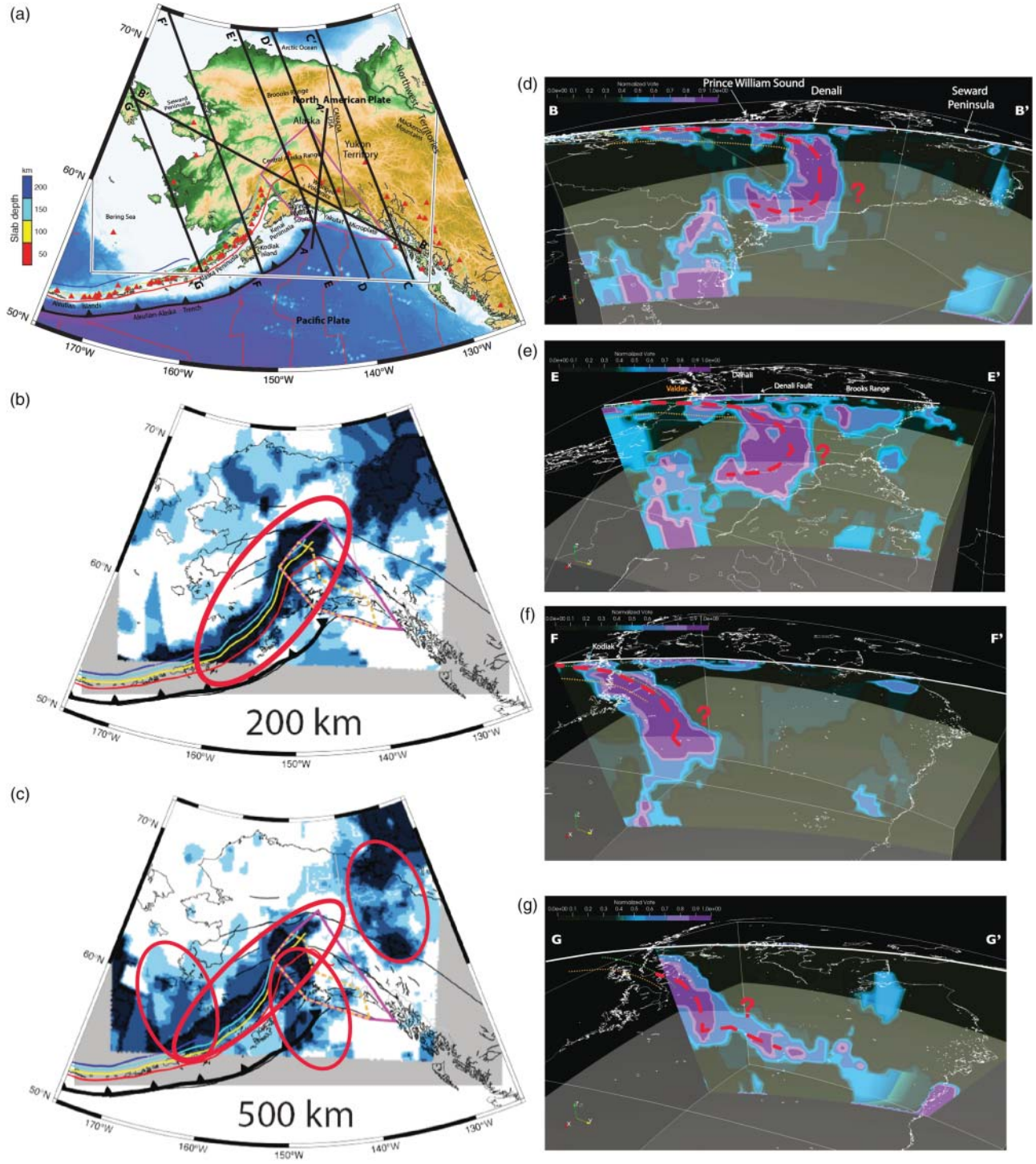

Figure 9.4 Slab and upper-mantle votemaps from Pavlis et al. (2024). (a) Location map with an outline of the seismic synthesis study area (black box) and cross-section lines. Alaska EarthScope seismic synthesis normalized vote maps showing agreement of high-velocity regions for (b,c) two depth slices and (d,e,f,g) four cross-sections. Translucent spherical shell surface marks 410 km depth in cross-sections (d,e,f,g). Areas of interest discussed in the text are highlighted in red ovals (b,c). Possible slab connectivity marked in cross-section by dashed red lines (d,e,f,g). Figure modified from Pavlis et al. (2024). See the electronic supplement to Pavli et al. (2024) for files used to visualize the vote map data in Paraview.

of Alaska that coincides with a similar structure observed previously from a synthesis of global models by Shephard et al. (2017).

6. Below western mainland Alaska, there is a suggestion from the EarthScope results that the deeper slab structure changes to lying flat on the transition zone. That is, instead of bending south to connect to a lower-mantle anomaly below southcentral Alaska, the slab in the Bering Sea may flatten to lie nearly horizontally in the transition zone.
7. The EarthScope seismic models strengthen the geologic observation of established terrane boundaries in Alaska. Our companion chapter (Yang et al., 2024) indicates that the models are convergent in defining boundaries that have a strong correlation with terrane boundaries. These observations reinforce the established geologic model that southern Alaska is assembled from crustal-scale terrane fragments.

9.3. REVIEW OF CONTINUUM MODELING APPROACHES TO SUBDUCTION

Geodynamic modeling can help elucidate viable mechanisms to explain the large-scale structure and nuanced tectonic features observed in EarthScope studies of the Aleutian–Alaska subduction zone. However, it is not always clear to disciplines outside of geodynamics, which model is applicable in a given setting or how the model design or governing equations may limit the applicability of that model to a given tectonic process. Thus, this section provides a brief overview of modeling approaches to subduction, with a focus on the application of continuum models to different parts of the subduction system. Implications for the Aleutian–Alaska subduction zone are then described in Section 9.4.

A number of review papers have summarized various aspects of geodynamic modeling as it relates to subduction systems, including slab dynamics (Billen, 2008), subduction modeling (Gerya, 2011, 2022; King, 2001), subduction parameters (Schellart, 2023), mantle flow in subduction zones (Jadamec, 2016a), numerical methods and workflows (Crameri, Schmeling, et al., 2012; Jadamec, 2016a; Müller et al., 2018; Van Zelst et al., 2022; Zhong et al., 2015), analog modeling (Schellart & Schellart, 2016), interactions with the transition zone (Goes et al., 2017), subduction initiation (Stern & Gerya, 2018), and seismic anisotropy within the slab and mantle (Karato et al., 2008; Long, 2013; Long & Becker, 2010). It is beyond the scope of this chapter to provide a new comprehensive review of subduction modeling. Thus, we direct the reader to these studies. A common theme in all of these papers is that the timescale of tectonic process being studied plays a key role in the selection of the kind of model being used, and importantly the governing physics and constitutive equations therein (Billen, 2008; Gerya, 2022; King, 2001; Moresi & Solomatov, 1995; Schellart & Strak, 2016; Van Zelst et al., 2022; Zhong, 2006; Zhong et al., 2015). Thus, in practice, many geodynamic modeling studies are grouped by the timescale of deformation and requisite governing equations, much as different seismic studies can be grouped by common methods or wave types being measured and analyzed.

When modeling the long-term deformation of the lithosphere, asthenosphere, and lower mantle, it is common to take a continuum modeling approach, wherein the solid-state creeping flow of the mantle can be approximated by the governing equations for incompressible viscous flow with the boussinesq approximation (Billen, 2008; Jadamec, 2016a; Kronbichler et al., 2012; Moresi & Solomatov, 1995; Zhong, 2006; Zhong et al., 2015). Even within the continuum approach, however, the domain over which the model is applied, and the questions being investigated, can result in substantively different models, in terms of model design, theoretical assumptions, rheology, tectonic process applicability, and computational resources and runtimes (Crameri, Tackley, et al., 2012; England et al., 1985; Fraters et al., 2019; Gerya, 2022; Gurnis et al., 2012; Jadamec, 2016a; Jadamec et al., 2012; Kaminiski & Ribe, 2002; Kronbichler et al., 2012; Moresi & Solomatov, 1995; Rudi et al., 2015; Sharples et al., 2014; Van Zelst et al., 2022; Zhong et al., 2015). Figure 9.5 illustrates common continuum subduction modeling types and the regions of the Earth over which they are typically applied. These models range from solving for deformation of a sheet of lithosphere to solving for deformation of the lithosphere, slab, and mantle within a large-scale mantle convection system (Figure 9.5). Note that the images in Figure 9.5 depict 3-D model domains, but many subduction modeling studies have been historically two-dimensional (2-D) models (Garfunkel et al., 1986; Jadamec et al., 2016b; Sobolev & Babeyko, 2005; Syracuse et al., 2010; van Keken et al., 2008), which can also provide valuable insight into tectonic process and mechanisms. We next describe these general modeling categories, highlighting models that have specific applications to the Aleutian–Alaska system.

Continuum models that simulate deformation restricted to the outermost portion of the Earth ($\lesssim$ 150 km depth), thus solving for deformation of the lithosphere (Figure 9.5), come in multiple forms that vary in the assumptions/simplifications for the continuity equations and model geometry (Bird & Piper, 1980; England et al., 1985; England & McKenzie, 1982; Flesch et al., 2001; Koons et al., 2010; McConeghy et al., 2022). These include, for example, thin viscous sheet, thin shell, spherical shell models, or just continuum models with a very shallow depth extent. Thin sheet viscous models (Figure 9.5) typically solve the conservation of mass and

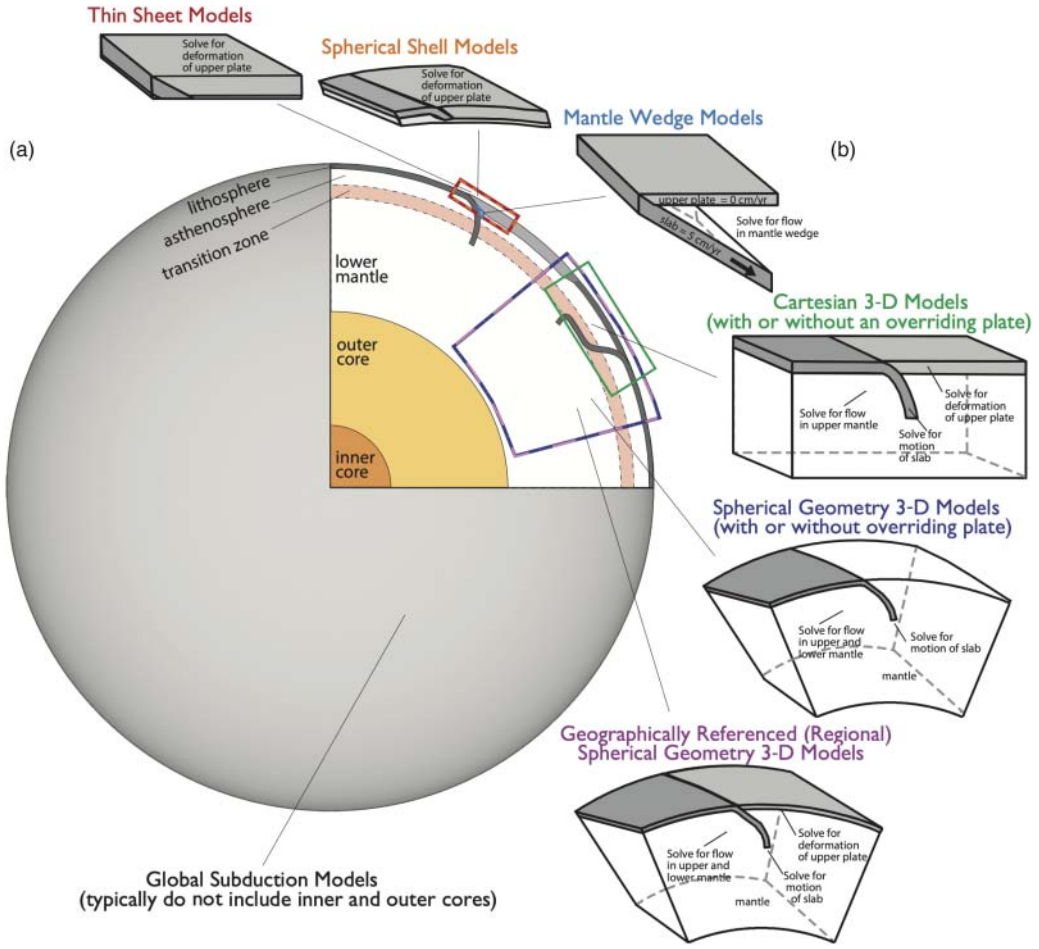

Figure 9.5 Schematic diagram of common approaches and regions of the Earth spanned by continuum models of subduction. (a) Spherical Earth diagram with internal rheological layers drawn to scale using 1215.0, 3485.0, 5710.8, 5960.8, 6170.8, 6270.8, and 6370.8 km for the radial length outward from the center of the Earth to the top of the inner core, top of the outer core, base of the transition zone, top of the transition zone, base of the continental lithosphere, base of the oceanic lithosphere, and surface of the Earth, respectively. From the surface of the Earth inward, these are 0, 100, 200, 410, 660, 2885.8, 5155.8, and 6370.8 km, respectively. Values for a radius of Earth with equal volume, inner core radius, and outer core radius are from Turcotte and Schubert (2014). An average value of 100 km for oceanic lithosphere and 200 km for continental lithosphere are used. (b) Inset diagrams showing typical extent of model domains for a given model type, with increasing domain size going clockwise around the arc. Inset diagrams are not drawn to scale. Note that this is not an exhaustive list of continuum model types, and in some cases the different models can be coupled through some form of output–input pipeline.

momentum equations for a viscous fluid, but assume the horizontal velocity is independent of depth, and are applied over a relatively thin domain (~100 km of the Earth) (Bird & Piper, 1980; England et al., 1985; England & McKenzie, 1982). The thin sheet style models solve for deformation of the lithosphere, by design, but do not solve the viscous equations for convection in the mantle, or the slab evolution (Figure 9.5). Such models have been applied to examine lithospheric deformation in the India-Asia collision zone (Bird & Piper, 1980; England et al., 1985; England & McKenzie, 1982), with a modified approach (Flesch et al., 2001) also applied to modeling lithospheric deformation in Alaska (Finzel et al., 2015). Spherical shell models (Figure 9.5) can be in different forms, but generally solve the conservation of mass and momentum for viscous flow for a thin curved outer layer or layers of Earth (~150 km), but without the restriction of the thin sheet models. Spherical shell models solve for lithospheric deformation, but do not solve the conservation equations for the slab dynamics, buoyancy-driven asthenospheric flow, or mantle convection (Figure 9.5). Recent thin shell models for Alaska solved for deformation of the upper 125 km of the Earth, with a horizontal velocity boundary condition applied to the underside of the model shell to

represent a mantle flow field (McConeghy et al., 2022). In addition, thermo-mechanical models with a Cartesian geometry, and model depth to 50 km, examined implications for plateau subduction and the effects of erosion on deformation in the Alaska plate boundary corner (Koons et al., 2010). We also point out earlier studies that examined upper plate deformation in Alaska, but also examined the trade-offs with fault configurations, using thin shell continuum elements (Bird, 1996; Kalbas et al., 2008).

The next general category of continuum subduction models is mantle wedge flow models (Figure 9.5). These models solve for the viscous flow in the mantle wedge and are typically referred to as corner flow models when in 2-D (Ribe et al., 2007; Turcotte & Schubert, 2014; van Keken et al., 2008; Wada et al., 2015). These models typically fix the upper plate and prescribe a downgoing plate speed as a boundary condition on an inclined slab of fixed orientation, and solve for the evolving flow (velocity and pressure) and temperature by solving the conservation of mass, momentum, and energy in the bounded mantle wedge corner (Figure 9.5). These models, thus, do not solve for upper plate deformation or convection of the mantle outside of the wedge. 2-D (Abers et al., 2006; Syracuse et al., 2010) and 3-D (Kneller & van Keken, 2008) mantle wedge models have shed light on the wedge thermal structure and flow for segments of the Aleutian–Alaska subduction zone, as well as for subduction zones worldwide (Syracuse et al., 2010).

The next continuum modeling category is grouped as generalized Cartesian or spherical viscous flow models of subduction (Figure 9.5) that solve the conservation of mass and momentum for the velocity and pressure, and may also solve the conservation of energy for the temperature if evolving the thermal field, with a model depth that extends to the transition zone and possibly lower mantle (Billen & Gurnis, 2007; Stegman et al., 2010; Zhong, 2006; Zhong et al., 2015). Thus, these models may solve the conservation equations for the viscous flow in the lithosphere, slab, and mantle (Figure 9.5). As the model domain is much larger, and hence more numerically expensive, the models may not include an overriding plate, may drive the slab velocity, and the Cartesian models typically are limited in depth to the transition zone because of the associated lateral limitations of the Cartesian configuration (Figure 9.5). 2-D generalized models with a Cartesian geometry examined the effects of plateau size and eclogitization with depth, with implications for plateau subduction in Alaska (Arrial & Billen, 2013).

Geographically referenced 3-D regional subduction models (Figure 9.5) also solve the conservation of mass, momentum, and energy (when evolving the thermal field) equations for the lithosphere, slab, and mantle dynamics, but are distinguished by incorporating the natural geometric complexity of a given tectonic system (Billen et al., 2003; Jadamec & Billen, 2016b; Moresi & Gurnis, 1996). 3-D geographically referenced instantaneous models of the Alaska subduction system have examined the effect of mantle flow and dynamic topography in the Aleutian segment (Billen & Gurnis, 2003), surface motions and slab-driven 3-D mantle flow beneath Alaska (Jadamec & Billen, 2010, 2012), the role of flat slab subduction and the Denali Fault shear zone in upper plate deformation in Alaska (Haynie & Jadamec, 2017; Jadamec et al., 2013), and simplified plateau subduction on deformation in Alaska (Haynie, 2019; Haynie & Jadamec, 2024). Note that the computational resources required are significantly larger for the large-scale 3-D geographically referenced models, which can extend to 1500 km depth costing 15,000 to over 30,000 CPU hours per job (Haynie, 2019; Haynie & Jadamec, 2017; Haynie & Jadamec, 2024; Jadamec & Billen, 2010, 2012; Jadamec et al., 2012, 2013).

Global models (Figure 9.5) can be spherical shell models spanning the circumference of the Earth, but only incorporating a thin outer domain (such as to model the lithosphere only), or can be larger-scale global models that solve the conservation equations for viscous flow over a domain that extends to the base of the lower mantle (Alisic et al., 2012; Conrad & Lithgow-Bertelloni, 2006; Faccenna & Becker, 2010; Zhong et al., 2000). For example, global models with observationally based slab geometries examined the effect of composite viscosity and yield stress on subduction and assessed the impact on plateness criteria, including for the Pacific Plate (Alisic et al., 2012). As global models may incorporate many subduction zones, it is not feasible to list every global model that contains the Aleutian–Alaska subduction zone. Note also that the resolution and details of subduction complexity will also vary from one model to the next.

In addition, in all cases, the length of time the model is run will vary depending on the hypotheses being examined and/or the computational constraints. In instantaneous models, for example, the conservation of mass and momentum equations is solved, but the conservation of energy is not, with the instantaneous models solving for snapshot in time (Billen et al., 2003; Jadamec & Billen, 2016b; Stadler et al., 2010). Alternatively, there can be time-dependent models that do not solve the conservation of energy or evolve the temperature, but still simulate the flow dynamics over time, for example, Stegman et al. (2006). Thus, it is important to read the methods in any given modeling paper to determine the resolution and timescales simulated to assess the applicability of any given model to a given tectonic process or process duration.

Lastly, we point out that there are numerous other kinds of models not described here. Numerical modeling is a

vast field. Specifically, we point out that kinematic-only models of Alaska (Elliott & Freymueller, 2020) are not described, nor are elastic dislocation models or tsunami models for Alaska (Suleimani & Freymueller, 2020; Zweck et al., 2002), for example. Although this section is focused on solid-state continuum models of subduction dynamics, other kinds of Alaska specific models are included in the next section where they can help place context on the observational constraints and help frame future studies.

9.4. INSIGHTS FROM GEODYNAMIC MODELING

In this section, we consider generalized and regional geodynamic models to gain insights on driving mechanisms that may explain several key features observed in the large-scale seismic structure of the Aleutian–Alaska subduction zone.

9.4.1. Correlation Between Curvature of Aleutian–Alaska Trench, Trench Motion, and Possible Interaction of the Slab With the Transition Zone

In a subduction zone, a trench that migrates into the surface part of the subducting plate (i.e., away from the overriding plate) is generally referred to as a retreating trench (Figure 9.6a,b) (Funiciello et al., 2003; Funiciello et al., 2008; Giuseppe et al., 2008; Goes et al., 2017; Royden & Husson, 2006; Schellart, 2004; Schellart, 2010a; Sharples et al., 2014). In contrast, a trench that moves toward the overriding plate is generally referred to as an advancing trench (Figure 9.6a,c) (Funiciello et al., 2003; Giuseppe et al., 2008; Goes et al., 2017; Schellart, 2010a; Sharples et al., 2014). At depth, a slab that sweeps laterally in the asthenosphere backward toward the unsubducted part of the downgoing plate is referred to as a slab that is rolling back (Figure 9.6b) (Funiciello et al., 2003; Garfunkel et al., 1986; Kincaid & Griffiths, 2003; Z H. Li et al., 2014; Schellart, 2010a; Sharples et al., 2014). Whereas, the opposite morphology is a slab that folds forward bending toward the upper plate, which can also referred to as a slab roll-forward or slab rollover (Funiciello et al., 2008; Giuseppe et al., 2008; Schellart, 2010a; Schellart et al., 2008; Sharples et al., 2014).

Numerical and analog models of subduction suggest that there tends to be a dynamic connection between the sense of motion of the trench at the Earth's surface and the interaction of the slab at depth with the transition zone, the region separating the lower viscosity upper mantle from the higher viscosity lower mantle (Figure 9.6b,d and c,e) (Funiciello et al., 2003; Funiciello et al., 2008; Giuseppe et al., 2008; Holt et al., 2015; Z H. Li et al.,

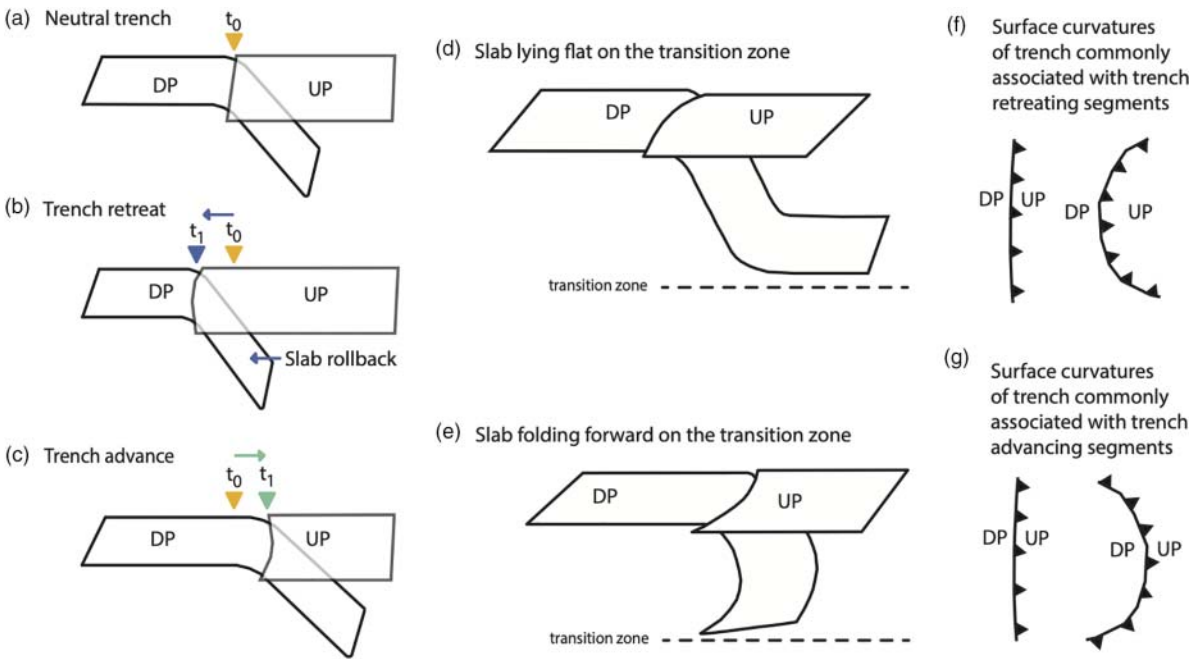

Figure 9.6 Schematic diagrams of (a–c) trench retreat and advance, (d, e) end-member transition zone interactions commonly associated with trench advance and retreat, and (f,g) segments of trench that may correlate with trench advance and retreat. DP, downgoing plate. UP, upper (overriding) plate. t_0 and t_1 refer to starting time and some time in the future, respectively. Inverted orange triangle denotes trench location at t_0, which is in the same location in panels (a)–(c). Diagrams based on synthesis of output from numerous numerical and analog models (Section 9.4.1). However, see Section 9.4.1 for factors affecting geometries.

2014; Schellart, 2004; Schellart, 2010a; Sharples et al., 2014). For example, geodynamic models suggest that slabs that lie flat on the transition zone tend to be associated with slab rollback within the mantle and trench retreat at the Earth's surface (Figure 9.6d) (Funiciello et al., 2003; Giuseppe et al., 2008; Z H. Li et al., 2014; Schellart, 2004; Schellart, 2010a; Sharples et al., 2014). Whereas, the models suggest that slabs that fold forward on the transition zone tend to be correlated with trench advance or a decreased rate of trench retreat at the Earth's surface (Figure 9.6e) (Funiciello et al., 2008; Giuseppe et al., 2008; Schellart, 2010a; Sharples et al., 2014).

In addition, numerical and laboratory geodynamic models suggest that there also tends to be a correlation between the sense of curvature of the trench and both the sense of motion of the trench and interaction of the slab with the transition zone (Schellart, 2010a; Schellart et al., 2007), but this can depend on a number of factors including the trench migration history, slab width, strength and density, upper plate properties, the presence of a lateral barrier, and slab–mantle viscosity ratio (Hale et al., 2010; Z H. Li et al., 2014; Schellart, 2004; Schellart et al., 2010a; Schellart et al., 2007; Stegman et al., 2006). For example, slabs that lie flat on the transition zone and undergo slab rollback and trench retreat, also tend to have a segment of the trench at the surface with a sense of trench curvature that is convex toward the downgoing plate (Figures 9.6b,d,f). In contrast, slabs that are folded forward on the transition zone and undergo trench advance tend to have a sense of curvature that is concave to the downgoing plate or that decreases in convexity toward the downgoing plate (Figures 9.6c,e,g) (Giuseppe et al., 2008; Schellart, 2010a). However, again, the slab and trench evolve through time, and the correlation can be affected by a number of factors, including the duration of subduction; the slab width, strength, and density; upper plate properties including thickness, slab–mantle viscosity ratio, motion of the downgoing plate, and the presence of lateral barriers (Funiciello et al., 2008; Giuseppe et al., 2008; Goes et al., 2017; Hale et al., 2010; Holt et al., 2015; Z H. Li et al., 2014; Schellart, 2005; Schellart, 2010a; Schellart et al., 2007; Sharples et al., 2014; Stegman et al., 2006).

In the central Aleutian segment of the Aleutian–Alaska subduction zone, the geometry of the trench is convex to the south, i.e., with the arc pointing toward the downgoing Pacific Plate (Figures 9.1 and 9.2) (Bird, 2003; DeMets et al., 1994; Hayes et al., 2018; Tozer et al., 2019). Based on generalized 3-D geodynamic modeling, this variation in trench geometry is what would be expected for trench retreat in the Aleutian segment. Depending on the reference frame, observations suggest that the Aleutian trench segment is indeed retreating (on the order of 1.9 to 2.4 cm/yr) or slightly advancing (0.1 cm/yr) (Schellart et al., 2008). This suggests that there could be rollback of the Pacific slab in the Aleutian segment of the subduction zone. It also suggests that if the slab were to extend to the transition zone in the Aleutians, it may be lying flat on the transition zone. A recent global compilation of slab–transition zone interaction geometries suggests that slab is lying flat on the transition zone in the Aleutian segment, but the resolution for slab connectivity in this region was limited (Goes et al., 2017). The recent EarthScope synthesis results for Alaska suggest that in the western region of the Alaska subduction zone segment, the slab may be lying flat on the transition zone (Figure 9.4g), which would be consistent with predictions from generalized geodynamic models. However, much work still needs to be done to confirm that this hypothesis is correct for the western Alaska segment, including both additional seismic studies to resolve the slab in the west and geodynamic models to test the effect of trench migration for the Aleutians.

In the eastern Alaska segment of the Aleutian–Alaska subduction zone, the trench geometry is concave to the south, i.e., with the arc opening toward the downgoing plate (Figures 9.1 and 9.2) (Bird, 2003; DeMets et al., 1994; Hayes et al., 2018; Tozer et al., 2019). Based on generalized 3-D geodynamic modeling, this is what would be expected for trench advance in the eastern Alaska segment or decreased trench retreat. Depending on the reference frame, synthesized observations indicate there is generally either decreased trench retreat in the Alaska segment or trench advance (Funiciello et al., 2008; Schellart et al., 2008). Thus, if the slab were to extend to the transition zone in the Alaska segment, this would suggest that the slab could be slightly lying flat, impinging on, or folded forward on the transition zone. This is consistent with the recent EarthScope synthesis results for the flat slab region of the Alaska subduction zone that suggest an eastward change in the slab interaction with the transition zone from lying flat, to impinging on, to folding over on the transition zone (Figure 9.4d–f). However, more data would need to be collected and time-dependent models run for Alaska to further test a causal connection between these observations for the Alaska case, especially in the eastern segment.

Similarly, relevant, global observations indicate that the magnitude of trench retreat for a subduction zone is typically greatest near the lateral terminations of the subduction zone (Schellart et al., 2007). However, this is not the case for the eastern termination of the Alaska subduction zone segment, where the observations indicate that the trench perpendicular retreat rate is decreasing, or the trench advance rate is increasing, depending on the reference frame (Funiciello et al., 2008; Schellart et al., 2008). Why then is the eastern termination of the subduction zone not undergoing significant trench

retreat? As indicated above, this could be due to the slab impinging on and folding forward on the transition zone in the eastern Alaska segment (Figure 9.4d–f), which could lead to a decrease in trench retreat rate or an increase in trench advance in this region. Alternatively, other factors could be at play. For example, it could also be due to the Yakutat plateau subduction-collision, wherein the positive buoyancy of the Yakutat terrane may prevent sinking of this upper portion of the slab and thus inhibit trench retreat. The observations that the Yakutat crust is relatively thicker in the eastern part of the plateau with a thickness up to on the order of 30 km in the offshore region could accentuate this effect (Christeson et al., 2010; Fuis et al., 2008; Haynie & Jadamec, 2024; Kim et al., 2014; Mann et al., 2022; Millet et al., 2023; Pavlis et al., 2019; Rondenay et al., 2010; Rossi et al., 2006; Worthington et al., 2012), as described in the next section.

9.4.2. Other Mechanisms for Curvature of Aleutian–Alaska Trench

Geodynamic models demonstrate there are other mechanisms that can also lead to variations in trench curvature, but that do not necessarily require the combined relation of trench curvature, trench motion, and slab–transition zone interaction as described in Section 9.4.1. For example, depending on the stage in the evolution of a given subduction zone, or depending on slab detachment processes, a given slab may not yet have reached the transition zone. In addition, in any given subduction zone, there may be lateral variations in physical properties in the subducting and/or overriding plates. However, many of the models, whose results are described in Section 9.4.1, were done without imposed along strike variations in the physical properties of the downgoing plate.

3-D models that contain along strike variations in downgoing plate properties provide an alternative explanation for trench curvature. The key physical property is lateral variations in the negative buoyancy of the slab. For example, a coupled finite element–boundary element model for the Aleutian–Alaska subduction zone, that allowed for trench motion, demonstrated that along strike changes in the tightness of curvature of the trench could be reproduced by taking into account the lateral variation in the seafloor age of the Pacific Plate (Morra et al., 2006). Here, decreased negative buoyancy of the slab from west to east along the downgoing plate led to a stronger slab with more slab pull in the west and a weaker slab with less slab pull in the east (Morra et al., 2006). These models produced a more steeply dipping slab and a more broadly curved convex-to-the-south trench in the west, and a more shallowly dipping slab and more tightly curved convex-to-the-south trench in the east (Morra et al., 2006). However, as a design simplification, the model does not contain an overriding plate or bounding plate on the east, where the North American Plate would be, thus the eastern boundary of the model has the Pacific Plate terminus simplified with respect to the observed subduction terminus in Alaska. In addition, the model did not test for the competing effects of plateau buoyancy. A separate study (Hale et al., 2010), using generalized 3-D finite-element models, produced a lateral decrease in trench retreat when testing the effect of a slab edge that terminated into a weak region representative of a transform fault, following the concept of a STEP fault subduction-transform boundary (Govers & Wortel, 2005), and varied the strength of the transform boundary. These models (Hale et al., 2010) showed that there is a lateral decrease in trench retreat rate where the slab approaches the transform boundary, and that the magnitude of retreat rate decreased with increasing strength along the transform boundary.

Another factor that has been found to influence trench geometry is the presence of thickened oceanic crust that characterizes oceanic plateaus (e.g., Mason et al., 2010) or the collision-subduction of continental material embedded within the oceanic plate, e.g., Magni et al. (2014). Generalized 3-D laboratory and numerical models of free subduction with an oceanic plateau or embedded continental blocks oriented at a high angle to a trench indicate that the shape of the trench becomes arcuate, with the curvature of the trench oriented convex in the direction away from the downgoing plate (Magni et al., 2014; Martinod et al., 2005; Mason et al., 2010). In addition, 3-D laboratory and numerical models predict that after a plateau is subducted, the uppermost part of the slab can shallow in dip to form a flat slab in the vicinity of the oceanic plateau, and the flanks of the slab then dip more steeply and away from the plateau (Martinod et al., 2005; Mason et al., 2010), resulting in a slab apex pointed in the direction of closure of a convex toward the upper plate trench geometry (Martinod et al., 2013), although not all of these models included an upper plate (Martinod et al., 2005; Mason et al., 2010). This curved flat slab apex geometry is consistent with that observed in the subducted plate beneath south central Alaska, where the flat slab is flanked by the more steeply dipping Aleutian portion of the slab to the west and the steeply dipping Wrangell slab to the east, with this curved-forward-to-the-northwest 3-D geometry of the flat slab region following the convex-to-the-north curvature of the trench in the eastern Alaska segment (Daly et al., 2021; Fuis et al., 2008; Gudmundsson & Sambridge, 1998; Jadamec & Billen, 2010, 2012; Mann et al., 2022; Page et al., 1989; Ratchkovski & Hansen, 2002b; Stephens et al., 1984; Wang & Tape, 2014; Zhao et al., 1995). More details on the slab geometry is discussed in Section 9.4.3.

More details on the upper plate deformation are described in Section 9.4.5, but it is important to point out that deformation within the upper plate can affect the position of the trench through time (Moresi et al., 2014; Schellart et al., 2008), which may be relevant for the Alaska section of the subduction zone in terms of terrane accretion and active deformation (Elliott & Freymueller, 2020; Moore & Box, 2016; Moresi et al., 2014).

9.4.3. Mechanisms of Flat Slab Subduction

As indicated above, the subduction of an oceanic plateau could lead to a very shallowly dipping or flat slab in 2-D or a very shallowly dipping or flat slab with an apex-like geometry in 3-D. However, there are a variety of factors that can lead to the formation of a flat slab segment in a given subduction zone, which do not require an oceanic plateau (Boutelier et al., 2003; Morra et al., 2006; Rodríguez-González et al., 2012; Sharples et al., 2014; van Hunen et al., 2002; van Hunen et al., 2004). Thus, when investigating a flat slab segment of a subduction zone, such as the eastern Alaska segment of the Aleutian–Alaska subduction zone, it is important to consider which of these factors, or combination of factors, may play a role.

Mechanisms leading to flat slab subduction can broadly be categorized into factors that relate to:

1. the downgoing plate buoyancy, such as subduction of a plateau, aseismic ridge, very large seamount, or young seafloor (Figure 9.7a,b)
   (Arrial & Billen, 2013; Espurt et al., 2008; Martinod et al., 2005; Mason et al., 2010; Morra et al., 2006; van Hunen et al., 2002);
2. the upper plate, such as an advancing upper plate or thick upper plate (Figure 9.7d,e)
   (S. Liu & Currie, 2016; Sharples et al., 2014; Sobolev & Babeyko, 2005);
3. the slab intersecting various kinds of boundaries, such as folding of the slab on the transition zone or subducting in a plate boundary corner (Figure 9.7c,f) (Funiciello et al., 2003; Schellart, 2004; Sharples et al., 2014); and
4. hydrodynamic forces, such as trench suction and asthenospheric flow (not shown in Figure 9.7) (Garfunkel et al., 1986; Tovish & Schubert, 1978);

or some combination of these factors (e.g., Manea et al., 2012; Rodríguez-González et al., 2012). In any given tectonic setting, the relative impact of these factors would have to be assessed with respect to the magnitude of the driving and resisting forces for that given setting at that point in the system's evolution (Arrial & Billen, 2013; Cloos, 1993; Manea et al., 2012; Mason et al., 2010). This includes the size of, as well as degree of metamorphic phase changes within, thickened features on oceanic crust, such as oceanic plateaus, aseismic ridges, seamounts, and island arcs (e.g., Cloos, 1993).

In the Aleutian–Alaska subduction zone, a number of tectonic features, predicted in subduction models that can cause flat slab subduction, occur in the location of shallow to flat slab subduction. For example, in terms of factors in the downgoing plate (Figure 9.7a,b), both subduction-collision of the Yakutat plateau and an eastward decrease in seafloor age occur in the shallow to flat slab region of the eastern Alaska segment of the subduction zone (Figures 9.1a and 9.2a). Factors with respect to boundaries (Figure 9.7f) include the recent EarthScope data that suggest the slab may be folded over on the transition zone (Figure 9.4d,e) (Pavlis et al., 2024), which could lead to a flat slab beneath south central Alaska. In addition, the eastern boundary of the subduction zone

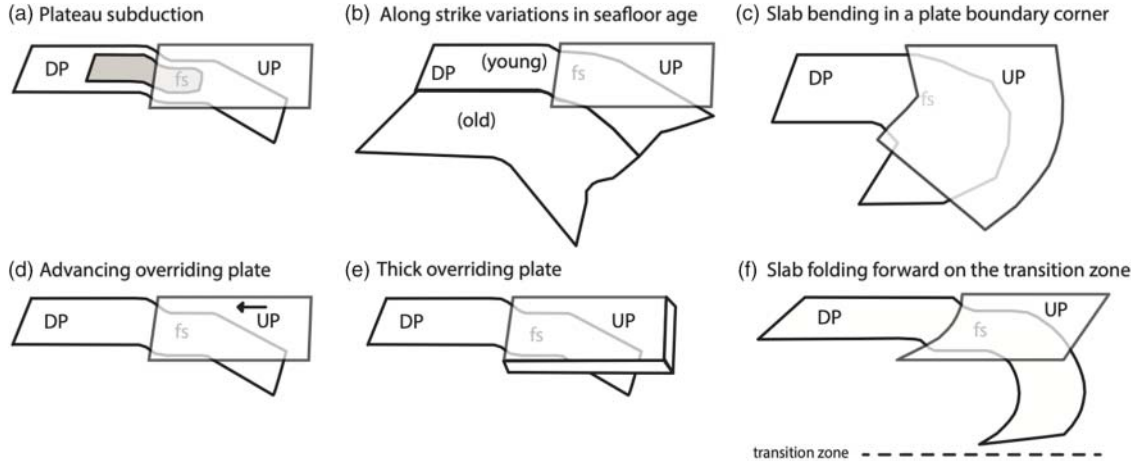

Figure 9.7 Schematic diagrams of factors in the downgoing plate (a,b), overriding plate (d,e), and boundary interactions (c,f) that can lead to flat slab subduction. Other factors such as hydrodynamic forces (trench suction) are not shown. DP, downgoing plate. UP, upper (overriding) plate. fs, flat slab segment. Diagrams based on synthesis of output from numerous numerical and analog models (Section 9.4.3). See Section 9.4.3 for discussion.

subducts into a plate boundary corner (Figures 9.1a, 9.2a and 9.7c) (DeMets et al., 1994; Jadamec & Billen, 2016b; Plafker, Moore, & Winkler, 1994). In terms of first-order overriding plate properties (Figure 9.7e), there is a change from ocean–ocean subduction in the western part of the Aleutian–Alaska subduction zone to ocean–continent subduction in the eastern segment (Figures 9.1 and 9.2) (Müller et al., 2019; Seton et al., 2020). However, the observed subduction zone geometry in the flat slab region (Fuis et al., 2008; Hayes et al., 2018; Jadamec & Billen, 2016b; Jadamec et al., 2018b; Veilleux & Doser, 2007), including constraints from recent EarthScope studies (Mann et al., 2022; Yang et al., 2024), suggest the upper plate is currently relatively thin above the flat slab region, despite it being an ocean–continent subduction zone. This suggests the Alaska flat slab segment of the Aleutian–Alaska subduction zone is in the category of flat slabs with very little mantle lithosphere in the overriding plate (Jadamec & Billen, 2012; X. Liu & Currie, 2019).

Thus, the previous models suggest that interactions with the transition zone, along strike variation in seafloor age, proximity to a transform boundary, and the subduction-collision of an oceanic plateau could all contribute to the trench morphology and slab morphology observed in the Alaska–Aleutian subduction zone. Therefore, it is important to test the relative effects of thermal buoyancy (density variation due to temperature changes) versus compositional buoyancy (density variation due to rock type and thickness), as well as interactions with the transition zone. Additional large-scale 3-D high-resolution models of Alaska, similar to that in Jadamec & Billen (2010, 2012), Jadamec et al. (2013), and Haynie & Jadamec (2017, 2024) (Figure 9.8), but with a migrating trench, would be beneficial to test new constraints on how a deeper slab geometry indicated by the EarthScope results could affect the time-dependent subduction evolution and trench geometry. (1) For example, large-scale 3-D models of Alaska extending to 1,500 km depth, used over 10 data sets to constrain the slab geometries used in their model, including Wadati Benioff zone seismicity, Vp and Vs data, and seismic reflection studies (Haynie & Jadamec, 2017; Jadamec & Billen, 2010, 2012; Jadamec et al., 2013). However, the slab geometry deeper than 300 km was less constrained at

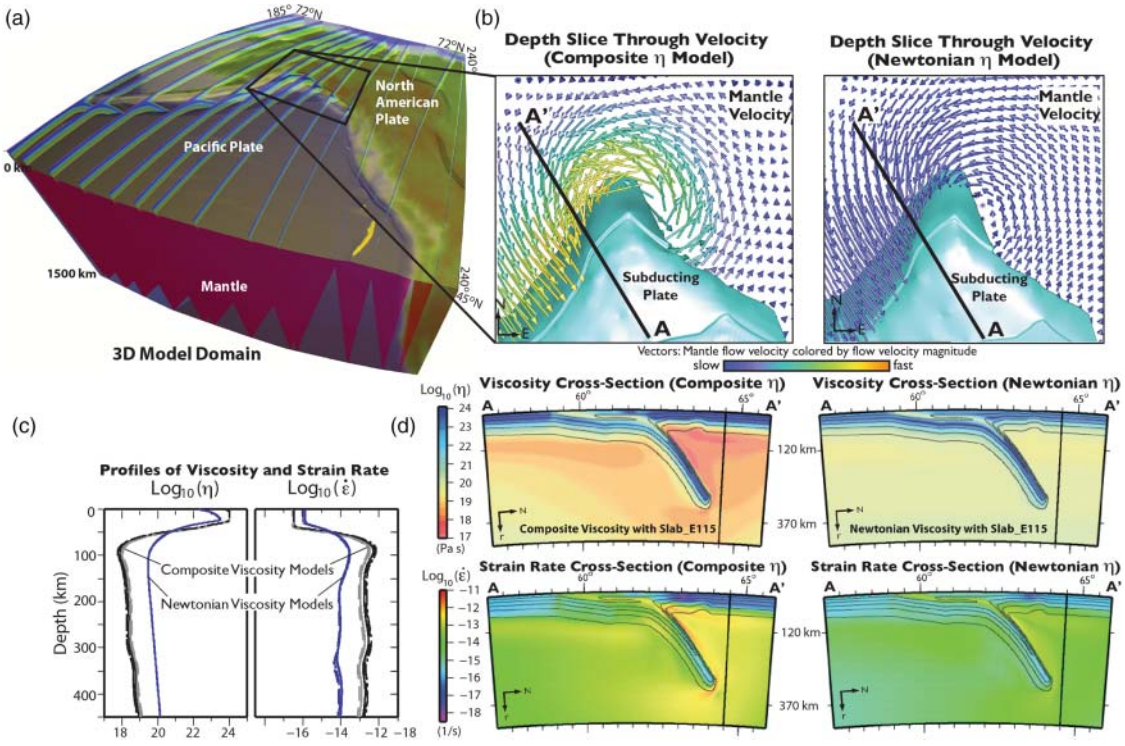

Figure 9.8 Three-dimensional, geographically referenced continuum models of Alaska showing toroidal flow around the eastern Alaska slab edge for two different mantle rheologies. (a) Domain of finite-element model, including cross-sections through initial thermal structure with variable plate thickness (Jadamec & Billen, 2010, 2012; Jadamec et al., 2012). Models use the Slab_{E115} geometry (Jadamec & Billen, 2010, 2012). Model domain depth is 1500 km. Topography draped on model surface shows model lateral extent. (b) Athenospheric flow velocity for models using composite (left) and Newtonian (right) upper-mantle viscosity at approximately 225 km depth for subset of model domain outlined by black box in (a). Modeled viscosity and strain rate in (d) cross-section AA′, with (c) corresponding profiles from vertical lines in (d). Figure modified from Jadamec & Billen (2010, 2012).

the time. Thus, although the EarthScope results suggest that the slab geometry at shallower depths is similar to that used in the geodynamic models of Jadamec and Billen Jadamec & Billen (2010, 2012), Jadamec et al. (2013), and Haynie & Jadamec (2017), the new EarthScope results suggest that the dynamic effects of a deeper slab geometry should also be tested. (2) In addition, previous large-scale models of Alaska examined the modern tectonics, solving for the instantaneous flow (Figures 9.8 and 9.9) (Haynie & Jadamec, 2017; Jadamec & Billen, 2010, 2012; Jadamec et al., 2013), and thus new models would be needed to study the time-dependent motion of the trench, which as noted above could be an important factor when examining the long-term evolution of the system. (3) Recent models have incorporated a simplified subducted plateau geometry onto the baseline 3-D geographically referenced models of Alaska (Haynie, 2019; Haynie & Jadamec, 2024) providing first-order constraints on the relative effect of the Yakutat plateau. New models would benefit from incorporating the offshore buoyancy of Yakutat microplate lithosphere, as well as incorporating a more geometrically complex plateau configuration (Haynie, 2019; Haynie & Jadamec, 2024; Pavlis et al., 2019). For example, active and passive seismic results across the Yakutat microplate reveal the eastward thickening wedge shaped crust of an oceanic plateau, spanning less than 10 km thick at its western end to on the order of 30 km thick at its eastern offshore end (Brocher et al., 1994; Christeson et al., 2010; Coulson et al., 2018; Eberhart-Phillips et al., 2006; Ferris et al., 2003; Fuis et al., 2008; Kim et al., 2014; J. Li et al., 2013; Mann et al., 2022; Pavlis et al., 2019; Worthington et al., 2012), with a synthesis in Haynie (2019) and Haynie and Jadamec (2024). Modeling that lateral variation in the Yakutat structure combined with observed downstream tear(s) will require increased computational resources (Haynie, 2019; Haynie & Jadamec, 2024). (4) In addition, the kinematic model of Fuston and Wu (2020) for the "Yukon slab" linked to Kula subduction and the kinematic model in our companion chapter (Pavlis et al., 2024) need to be tested with more a physics-based model.

9.4.4. Plateau Subduction, Possible Detachment of the Wrangell Slab, and Implications for Mantle Flow

Geodynamic models indicate that on long timescales subducted lithosphere can behave viscously (Billen & Hirth, 2004; Cizkova et al., 2002), and when stressed, the subducted lithosphere can attenuate leading to partial or full slab detachment (Burkett & Billen, 2009, 2010; Gerya et al., 2004; L. Liu & Stegman, 2012). For example, time-dependent models of plateau subduction indicate the flat slab geometry can evolve with time and can result in distortion that can lead to disruption of the slab (Mason et al., 2010; Vogt & Gerya, 2014). For flat slabs associated with the subduction of thick oceanic plateaus and aseismic ridges or very large seamounts, the positive compositional buoyancy from the overthickened crust can lead to lithosphere that is positively buoyant (Figure 9.7a), causing spatial and temporal changes in slab morphology (e.g., van Hunen et al., 2002). In three dimensions, this can result in an apex forming in the slab with the crest of the apex coincident with the plateau during some point in the slab evolution (Espurt et al., 2008; Martinod et al., 2005; Mason et al., 2010). The resistance to subduction can also lead to partial separation of the slab (Mason et al., 2010) or result in complete slab detachment (Vogt & Gerya, 2014). Geodynamic models also indicate, however, that thickened downgoing plate material can be subducted to depths of several hundred kilometers (Arrial & Billen, 2013; Boutelier et al., 2003; van Hunen et al., 2002) and result in continuous subduction without slab detachment.

Based on plate motions and subduction in the northern Pacific during the Cenozoic, mass conservation sugests that a slab would be expected to be present to the 660 km discontinuity beneath Alaska (Eberhart-Phillips et al., 2006; P J. Haeussler et al., 2003; Lonsdale, 1988; Madsen et al., 2006; Qi et al., 2007; Sdrolias & Müller, 2006; W. Wallace & Engebretson, 1984), and therefore, it would be expected that a deeper slab would extend laterally farther east of the flat slab apex (into the Wrangell slab region) than implied by the distinct reduction in seismicity at 212◦ longitude (Daly et al., 2021; Fuis et al., 2008; Ratchkovski & Hansen, 2002b; Stephens et al., 1984; Zhao et al., 1995; Veilleux & Doser, 2007). In addition, 3-D instantaneous geodynamic simulations that tested the impact of two slab geometries on the dynamics of mantle flow and upper plate deformation in Alaska found that the model with a short Wrangell slab east of the flat slab apex produced a better fit to observations (Jadamec & Billen, 2010, 2012). Thus, the seismicity and seismic tomography observations (Daly et al., 2021; Fuis et al., 2008; Hayes et al., 2018; Ratchkovski & Hansen, 2002b; Stephens et al., 1984; Ward & Lin, 2018; Yang & Gao et al., 2020; Zhao et al., 1995), as well as the agreement between the infinite strain axes produced by the 3-D mantle flow field (Jadamec & Billen, 2010, 2012) and independent observations of shear-wave splitting (Christensen & Abers, 2010), suggest that a short Wrangell slab east of the slab apex is closer to reality, with earlier as well as recent EarthScope seismic studies suggesting slab segmentation in this region and possibly a tear(s) of various sizes (Fuis et al., 2008; Jadamec & Billen, 2010, 2012; Mann et al., 2022; Pavlis et al., 2019; Ratchkovski & Hansen, 2002b; Stephens et al., 1984; Veilleux & Doser et al., 2007; Yang & Gao, 2020; Zhao et al., 1995).

This leads to the question of whether there was either an intrinsically short (~115 km) slab segment east of the flat slab apex beneath the Wrangells since initiation, for reasons not yet understood, or did the deeper part of the Wrangell slab on the east side of the Yakutat plateau undergo slab detachment? In addition, if there was slab disruption and detachment, was it limited to a single episode or could there have been multiple episodes of tearing? Also, could the newly discovered "Yukon River Anomaly" be the a relic of the slab prior to the development of a slab tear? The geodynamic feasibility of these questions for the Alaska-specific case remains to be tested. New instantaneous models would benefit from incorporating the deeper slab segments suggested by the new EarthScope data to examine the effect on the instantaneous dynamics, and time-dependent models can use these new slab location observations as constraints on differing forward modeling simulations that incorporate evolving slab morphologies and trench motion. Previous studies have suggested that the subduction of the remains of the failed Kula-Farallon spreading center could create complexities in the system (Madsen et al., 2006; Qi et al., 2007). However, west of the Wrangell slab, the recent EarthScope data (Pavlis et al., 2024) suggest that the Pacific slab may be continuous to the transition zone, with a geometry that may be folded forward beneath south central Alaska and laying flat on the transition zone in the western part of the Alaska subduction zone segment (Figure 9.4). Again, future 4-D models and seismic studies will be required to further examine this process for Alaska.

Lastly, it is also important to point out that geodynamic models demonstrate that the motion of the slab, either as an intact entity or as a feature that has undergone attenuation and partial or full slab detachment, will have an impact on the local flow dynamics of the asthenosphere (e.g., Jadamec, 2016a), including driving complex flow patterns around or through the slab (Burkett & Billen, 2009, 2010; Gerya et al., 2004; Jadamec & Billen, 2012; Kincaid & Griffiths, 2003; Kiraly et al., 2020; Leo et al., 2014; L. Liu & Stegman, 2012; MacDougall et al., 2014; Magni et al., 2014; Paczkowski et al., 2014). Geodynamic modeling, rock deformation experiments, and seismic observations indicate that model-predicted flow fields in the upper mantle and associated predicted lattice preferred orientation of olivine, for example, can be constrained by independent seismic observations of shear-wave splitting wherein mantle deformation fabrics can split shear waves resulting in a fast azimuth that can subparallel the flow direction and a splitting delay time indicative of the intensity or pervasiveness of the deformation fabric (Faccenda & Capitanio, 2012; Fischer et al., 2000; Jadamec & Billen, 2016b; Kaminiski & Ribe, 2002; Karato et al., 2008; Kneller & van Keken, 2008; M. Long & Wirth, 2013; M D. Long & Becker, 2010; M D. Long and Silver, 2008; MacDougall et al., 2017; Savage, 1999). Thus, shear-wave splitting studies from the Aleutian–Alaska subduction zone (e.g., Christensen & Abers, 2010; Gou et al., 2019; Hanna & Long, 2012; McPherson et al., 2020; Perttu et al., 2014; Richards et al., 2021; Venereau et al., 2019), will be important for placing critical constraints on the mantle flow dynamics of the region, including slab-driven mantle flow (Billen & Gurnis, 2003; Jadamec & Billen, 2016b; Jadamec & Billen, 2012; Jadamec et al., 2018b; Kneller & van Keken, 2008; Rondenay et al., 2010) and plate–mantle coupling (Billen & Gurnis, 2003; Finzel et al., 2015; Jadamec et al., 2016a; Jadamec & Billen, 2010, 2012; McConeghy et al., 2022).

For example, 3-D instantaneous, geographically referenced regional models of the Alaska subduction-transform system produced toroidal flow in the asthenosphere around the eastern Alaska slab edge, with counterclockwise-directed flow moving from underneath the flat slab apex to below the shorter Wrangell slab and around the deeper Pacific segment into the mantle wedge in the vicinity of Denali (Figures 9.8 and 9.9) (Jadamec, 2016a; Jadamec & Billen, 2010, 2012; Jadamec et al., 2012). Predicted mantle deformation related to the toroidal flow was quantitatively compared (Jadamec & Billen, 2016b) to pre-EarthScope observations of shear-wave splitting (Christensen & Abers, 2010) and is consistent to a first order with more recent studies (Gou et al., 2019; Hanna & Long, 2012; McPherson et al., 2020; Perttu et al., 2014; Richards et al., 2021; Venereau et al., 2019). Located within the arc of the toroidal flow, the geodynamic models (Jadamec, 2016a; Jadamec & Billen, 2010, 2012) also produced localized slab-edge-driven vertical upwelling in the asthenosphere in the vicinity of the overlying Wrangell volcanics (Figures 9.8 and 9.9b), which may provide a mechanism for the anomalous geochemical signature and location of the Wrangell volcanoes (Brueseke et al., 2023; Brueseke et al., 2019; Jadamec, 2016a; Jadamec & Billen, 2010, 2012; Jadamec et al., 2018b; Preece & Hart, 2004; Skulski et al., 1991). This flow is consistent to a first order with null splits near the Wrangells (e.g., Hanna & Long, 2012). Generalized laboratory and numerical models of slab-edge-driven asthenospheric flow also predict localized mantle upwelling associated with the zone of toroidal flow around lateral slab edges (Funiciello et al., 2006; Jadamec, 2016a; Piromallo et al., 2006; Schellart, 2010b; Strak & Schellart, 2014; Stegman et al., 2006). The geodynamic models of Jadamec and Billen Jadamec and Billen (2010, 2012) were the first high-resolution models to simulate this localized mantle upwelling effect around the eastern slab edge in Alaska (Figures 9.8 and 9.9). If the Wrangell slab has undergone partial or complete slab detachment as well, then this process could be enhanced (Burkett & Billen, 2010; L. Liu & Stegman, 2012).

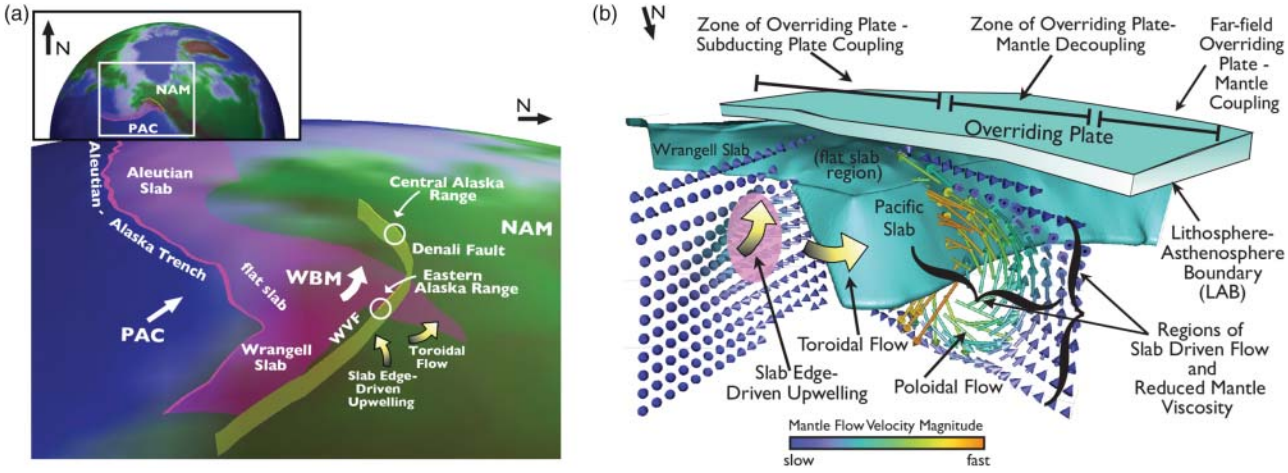

Figure 9.9 Geodynamic setting for the Alaska subduction zone with pre-EarthScope Slab*E*115 from Jadamec and Billen (2010, 2012). (a) Pacific–Wrangell slab geometry shown in magenta surface (Jadamec & Billen, 2010, 2012) and Denali Fault shown in yellow surface (Jadamec et al., 2013 and references therein). View to the west (toward the Aleutians). PAC, Pacific Plate with approximate motion vector in white. WBM, Wrangell Block microplate with schematic motion vector in white. NAM, inboard North American Plate. WVF, Wrangell volcanic field. (b) Pacific–Wrangell slab geometry and cross-sections through predicted 3-D flow velocity field in the asthenosphere from geodynamic models of Jadamec & Billen (2010, 2012) for subset of model domain. Yellow shaded arrows show schematic of model-predicted torodial flow and asthenospheric upwelling, with slices through modeled flow velocity field in the asthenosphere at approximately 250 km depth shown in Figure 9.8. Depth of Pacific slab thermal anomaly used in model is approximately 325 km in the west and 115 km beneath the Wrangells. A laterally variable upper plate is included in the models (Jadamec & Billen, 2010, 2012; Jadamec et al., 2013), although it is shown only schematically in the figure here. Note, the compositional buoyancy of Yakutat plateau is not included in these models. See Haynie and Jadamec (2024) for a recent synthesis on the Yakutat plateau. View looking to the southwest (toward the western Pacific Ocean). Figure modified from Jadamec and Billen (2010, 2012), Jadamec et al. (2013), and Jadamec (2016a).

Future 4-D models are needed to investigate possible slab detachment in Alaska due to the Yakutat plateau subduction-collision, and observations of shear-wave splitting will place important constraints on this process.

9.4.5. Overriding Plate Participation in and Response to Subduction

Flat slab subduction and the subduction of thickened oceanic crust have been shown to cause wide zones of deformation in the overriding plate that can extend hundreds of kilometers inboard (Bird, 2003; Espurt et al., 2008; Gutscher et al., 2000; Jadamec et al., 2013; Jarrard, 1986; Jordán et al., 1983; Martinod et al., 2013; Schellart, 2008; Sébrier et al., 1988). Previous models have shown that the slab can drive deformation in south central Alaska, on the order of several hundred kilometers from the plate boundary (Bird, 1996; Haynie & Jadamec, 2017; Jadamec et al., 2013; Koons et al., 2010; Mazzotti & Hyndman, 2002). The distribution of deformation can also be affected to a first order by the introduction of lithospheric heterogenieties (Haynie & Jadamec, 2017; Jadamec et al., 2013; Kalbas et al., 2008). For example, previous 3-D regional models, which extended to 1500 km depth and included thermal buoyancy driven deformation (Haynie & Jadamec, 2017; Jadamec et al., 2013), found that the combination of the flat slab and Denali fault could reproduce the first-order features in south central Alaska, such as the sense of motion of the Wrangell block, the location of the Central Alaska Range, the progression from strike slip to convergence along the Denali Fault, and the Cook Inlet and Sustina basins. More recent 3-D regional instantaneous models, which also extended to 1500 km depth, examined the relative contribution of the slab shape versus the additional compositional buoyancy of the shallow part of a plateau on the location, magnitude, and nature of the mountain building and basin formation in the overriding plate, as well as the ability of the downgoing plate to drive rotational motion of the upper plate in south-central Alaska (Haynie, 2019; Haynie & Jadamec, 2024). Thin sheet style models, incorporating the effect of lateral variations in gravitational potential energy to 100 km depth, produced widespread deformation throughout

Alaska and examined the effect of tractions on the base of the model but did not solve the viscous equations for flow within the underlying mantle (Finzel et al., 2015). More recent 3-D thin shell models, extending to 125 km depth, also demonstrated large-scale deformation across the lithosphere in Alaska and northwestern Canada (McConeghy et al., 2022).

One of the aspects of the Aleutian–Alaska subduction zone that the EarthScope syntheses results help to shed light on is the nature of how the differing tectonic components relate to one another in three dimensions (Figures 9.3 and 9.4). Specifically, as it relates to upper plate deformation, important findings include comparing seismic studies on the thickness of the crust and lithosphere in the overriding plate (Yang et al., 2024) (Figure 9.3) and how these depths relate to the location of the top of the slab/plateau, as well as the location of subducted continuous and/or discontinuous slab fragments embedded within the mantle (Pavlis et al., 2024) (Figure 9.4). The relative position of the flat slab with respect to the upper plate is important for quantifying the area of the subduction interface and how the nature of the overlap may influence upper plate deformation (Haynie & Jadamec, 2017; Jadamec et al., 2013; Sharples et al., 2014), as well as seismicity along the subduction interface (Christensen & Beck, 1994). In addition, the characterization of the deeper slab structure is important because stresses transmitted updip that can impact the deformation can depend on the nature of the slab interaction with the transition zone as well as slab strength (Goes et al., 2017). The location and geometry of the slab at depth, as well as the location of any slab remnants, are also important because of the possible impact on asthenospheric flow dynamics (Jadamec, 2016a; L. Liu & Stegman, 2012), which can result in dynamic topography in the upper plate (Jadamec et al., 2013). Moreover, geodynamic models indicate that not only do the slab properties play a key role in upper plate deformation, but also that upper plate properties such as plate thickness, strength, thermal structure, and density can in turn control the evolution of the slab and/or the subduction zone dynamics (Holt et al., 2015; Jadamec & Billen, 2012; Rodríguez-González et al., 2012; Royden & Husson, 2006; Sharples et al., 2014).

Thus, more work needs to be done to test the relative importance of the new features identified in the EarthScope results in a set of fully 3-D geodynamic models that allow for trench evolution, test a deep slab morphology, take into account the time-dependent subduction-collision of the Yakutat plateau, include the related phase transition from basalt to eclogite during the plateau subduction, as well as include elastic effects of the lithosphere (Bird, 1996; Finzel et al., 2011; Fitzgerald et al., 1993; Freymueller et al., 2008; P. Haeussler, 2008; Jadamec & Billen, 2016b; Jadamec et al., 2013; Kalbas et al., 2008; Kneller & van Keken, 2008; Koons et al., 2010; Lundgren et al., 1995; Mazzotti & Hyndman, 2002; Plafker, Gilpin, & Lahr, 1994; Plafker, Moore, & Winkler, 1994; Redfield et al., 2007; Rondenay et al., 2010; Schultz & Aydin, 1990).

9.4.6. Implications for Other Subduction Zones in the Pacific Ring of Fire

To place the Aleutian–Alaska subduction system and recent EarthScope results in a larger context, the large-scale similarities and differences between the Aleutian–Alaska system and the other subduction systems along the Pacific Ring of Fire are considered. There are a variety of global synthesis papers on tectonic features in modern subduction zones. For example, comparative analyses on subduction zone parameters examine slab dip (Hayes et al., 2018; Jarrard, 1986; Lallemand et al., 2005) with virtual movie collections (Jadamec et al., 2018a, 2018b) and interactive functionalities (Hayes et al., 2018), global data constraints on seafloor crustal age (Müller et al., 2019; Seton et al., 2020), the articulation of plate boundaries (Argus, Gordonand DeMets et al., 2011; Bird, 2003; DeMets, Gordonand Argus et al., 2010; DeMets et al., 1994), trench-perpendicular motion rates in different reference frames (Schellart et al., 2008), and observations of shear-wave splitting (Long & Wirth, 2013; Long et al., 2013). In the subsequent paragraphs, we highlight the large-scale tectonic features primarily with respect to the data plotted in Figures 9.1b and 9.2b, going counterclockwise along the Pacific Ring of Fire (DeMets et al., 1994; Hayes et al., 2018; Müller et al., 2019; Seton et al., 2020; Smithsonian, 2012; Tozer et al., 2019).

The Aleutian–Alaska subduction zone contains both ocean–ocean and ocean–continent subduction zone segments due to the lateral variations in upper plate lithosphere from west to east (Figures 9.1b and 9.2b) (Müller et al., 2019; Seton et al., 2020; Tozer et al., 2019). Other subduction zones along the Pacific Ring of Fire containing both large-scale ocean–ocean and ocean–continent subduction zone segments, going counterclockwise along the Ring of Fire, include (1) possibly the Middle America trench, (2) the Kurile–Kamchatka–Japan–Izu–Bonin–Marianas subduction zone, (3) the Solomon Islands Region, and (4) the Hikurangi–Tonga–Kermadec subduction zone (Figures 9.1 and 9.2) (Müller et al., 2019; Seton et al., 2020; Tozer et al., 2019). Note that plate-like behavior is scale-dependent, and there are many regions where there are broad zones of internal deformation in the upper plate (Argus et al., 2011; Bird, 2003; DeMets et al., 2010;

DeMets et al., 1994). This deformation can occur in multiple forms including large-scale intracontinental shear zones, distributed seismicity, and mountain building, e.g., Bird (2003), many of which are observed in mainland Alaska and northwestern Canada (e.g., J. A. Benowitz et al., 2022; Elliott & Freymueller, 2020; Fitzgerald et al., 2014; Fuis et al., 2008; Haynie & Jadamec, 2017; Koehler et al., 2018; Mazzotti & Hyndman, 2002; Ratchkovski & Hansen, 2002a).

The Aleutian–Alaska subduction zone is a partially isolated subduction zone, with the western end of the Aleutian–Alaska subduction zone intersecting with the northern terminus of the Marianas–Izu–Bonin–Japan–Kurile–Kamchatka subduction zone (Figures 9.1b and 9.2b) (DeMets et al., 1994; Hayes et al., 2018; Jadamec et al., 2018a, 2018b; Müller et al., 2019; Seton et al., 2020; Smithsonian, 2012; Tozer et al., 2019). Other major subduction zones terminating into another subduction zone forming an intersection, going counterclockwise along the Ring of Fire, include (1) the northern Nazca–southern Cocos subduction intersection/slab gap; (2) the Boso Triple Junction where the Ryukyu-Nankai subduction zone intersects the western Pacific slab (Marianas–Izu–Bonin–Japan–Kurile–Kamchatka subduction zone) under Japan; (3) the southern Ryukyu–Nankai and northern Manila slab intersection under Taiwan; (4) the Manila and Philippine slab overlap; (5) the southern Philippine, Halmahera, Sulawasi, northern Banda slab region; and (6) the Hikurangi and Puysegur slab polarity reversal region (Figures 9.1b and 9.2b) (DeMets et al., 1994; Hayes et al., 2018; Müller et al., 2019; Seton et al., 2020; Tozer et al., 2019). Note that the nature of the subduction–subduction intersections can be complex, including possibly abutting slabs or gaps between the slabs (Figures 9.1b and 9.2b) (DeMets et al., 1994; Hayes et al., 2018; Jadamec et al., 2018a, 2018b; Müller et al., 2019; Seton et al., 2020; Tozer et al., 2019). For example, plate kinematics suggest a slab gap related to the transition to strike-slip motion in the western most end of the Aleutian subduction zone where it intersects the northern Kamchatka subduction zone (DeMets et al., 1994; Hayes et al., 2018).

The eastern end of the Aleutian–Alaska subduction zone and the northern end of the Fairweather–Queen Charlotte transform boundary are oriented at a near-right angle, with the Yakutat plateau actively subducting-colliding into Alaska at this juncture (Figures 9.1b and 9.2b) (DeMets et al., 1994; Enkelmann et al., 2009; Hayes et al., 2018; Müller et al., 2019; Pavlis et al., 2019; Seton et al., 2020; Smithsonian, 2012; Tozer et al., 2019; W K. Wallace et al., 2008; Worthington et al., 2012). Other subduction zones that have a major transform boundary near their terminus, going counterclockwise along the Ring of Fire, include (1) Cascadia, (2) the Ryukyu–Nankai intersection with northern Manila under Taiwan in some cases is considered a transform intersection along the Longitudinal Valley Fault, (3) the eastern end of the New Hebrides subduction zone, (4) the northern end of the Tonga–Kermadec subduction zone, and (5) the Hikurangi subduction zone and the Alpine Valley Fault (this is also a subduction polarity reversal region) (Figures 9.1b and 9.2b) (DeMets et al., 1994; Hayes et al., 2018; Müller et al., 2019; Schellart et al., 2008; Seton et al., 2020; Smithsonian, 2012; Tozer et al., 2019). Note that there are additional locations that may also contain minor/short transform boundaries as part of accommodating the larger slab–slab and slab–rift intersections (Bird, 2003), which are not included in the list. Rather, the regions with large-scale plate boundary intersections are included but even within these large-scale boundaries there are in turn often local effects, including obliquity that can lead to nontranslational components of motion (Bird, 2003). When comparing and contrasting the subduction-transform zones, it is worth pointing out that the relative geometry of the intersections can vary. For example at the eastern Alaska subduction zone, the strike of the Aleutian–Alaska trench and the strike of the Fairweather–Queen Charlotte transform boundary are nearly perpendicular (Figures 9.1b and 9.2b) (DeMets et al., 1994; Hayes et al., 2018; Müller et al., 2019; Seton et al., 2020; Tozer et al., 2019). Whereas for the Cascadia trench–Queen Charlotte transform boundary intersection, the Cascadia trench–San Andreas transform boundary intersection, and the Hikurangi–Alpine fault boundary intersection, for example, the strike of the trench and the transform boundaries are subparallel (Figures 9.1 and 9.2) (DeMets et al., 1994; Hayes et al., 2018; Müller et al., 2019; Seton et al., 2020; Tozer et al., 2019). Regions also occurring with plateau subduction-collisions are described below.

There are oceanic seamounts, oceanic plateaus, and large igneous provinces (LIPs) distributed throughout the Pacific Ring of Fire (Bryan & Ferrari, 2013; Cloos, 1993; Tozer et al., 2019) (Figure 9.2b). These are commonly associated with thickened oceanic crust and localized elevated seafloor of varying degrees (Bryan & Ferrari, 2013; Tozer et al., 2019), but not all of these features will result in the disruption of a subduction zone (e.g., Cloos, 1993). In the western Aleutian–Alaska subduction zone, the intersection with the Kurile–Kamchatka subduction zone is along the trajectory of the Hawaiian-Emperor seamount track (Figure 9.2b) (Bryan & Ferrari, 2013; Tozer et al., 2019). In the eastern Aleutian–Alaska subduction zone, there is active subduction-collision of the Yakutat plateau coincident with large-scale deformation of the upper plate (Figure 9.2a) (Bruns, 1983; Eberhart-Phillips et al., 2006; Elliott et al., 2013; Enkelmann et al., 2010; Estabrook et al., 1992; Haynie & Jadamec, 2024; Koons et al., 2010;

Mazzotti & Hyndman, 2002; Pavlis et al., 2019; W K. Wallace et al., 2008; Worthington et al., 2012). Other locations along the Pacific Ring of Fire undergoing seamount, plateau/LIP subduction interaction, going counterclockwise along the Ring of Fire, include (1) the Peru–Chile segments of the Nazca subduction zone, (2) the Middle America trench and the Columbian section of the Nazca subduction zone associated with the Galapagos seamount track, (3) the Izu–Bonin–Marianas subduction zone, (4) the Ryukyu–Nankai subduction zone, (5) the northern Philippine subduction zone, (6) the Marianas–Yap subduction zone region, (7) the Solomon Islands Region, (8) the southern New Hebrides region, (9) the Tonga–Kermadec subduction zone, and (10) the Hikurangi and Puysegur subduction zones (Figures 9.1b and 9.2b) (Bryan & Ferrari, 2013; Cloos, 1993; Tozer et al., 2019). Where these buoyant subducting-colliding features are large, the result can be major disruption of the subduction zone, upper plate, and plate boundary position (e.g., Cloos, 1993; Moresi et al., 2014).

As described in the previous sections, Aleutian–Alaska subduction zone contains a sub-horizontal to flat slab segment in the eastern part of the subduction zone beneath south-central Alaska, that is spatially coincident with young seafloor offshore, subduction-collision of the Yakutat plateau, proximity to a plate boundary corner, and an ocean–continent subduction zone segment (Figures 9.1 and 9.2) (Fuis et al., 2008; Gou et al., 2019; Jadamec & Billen, 2016b; Jadamec et al., 2018b; Mann et al., 2022; Morra et al., 2006; Nayak et al., 2020; Pavlis et al., 2019; Ratchkovski & Hansen, 2002b; Veilleux & Doser, 2007; Worthington et al., 2012; Yang & Gao, 2020; Zhao et al., 1995). The flat slab geometry can be seen by the very wide spacing in the 20 km slab contours (Hayes et al., 2018) in south central Alaska, south of the Denali fault in the vicinity of Prince William Sound and the Kenai Peninsula (Figures 9.1a and 9.2a). Other locations along the Pacific Ring of Fire with subhorizontal to flat slab segments going counterclockwise along the Ring of Fire include (1) portions of the Chile and Peru segments of the Nazca subduction zone, (2) part of the Mexico segment of the Cocos subduction zone, (3) part of Cascadia, and (4) part of the Japan subduction zone (Figures 9.1b and 9.2b) (Gutscher et al., 2000; Hayes et al., 2018; Lallemand et al., 2005). Note that a key difference with the Alaska subhorizontal to flat slab segment is that the slab begins shallow very close to the trench, and thus there is very thin (0–40 km) upper plate above flat slab in Alaska (Fuis et al., 2008; Hayes et al., 2018; Jadamec & Billen, 2016b; Mann et al., 2022; Zhao et al., 1995). In contrast, in Chile and Peru, for example, the subhorizontal to flat slab segment does not start until at least 80 km depth (Figures 9.1b and 9.2b) (Hayes et al., 2018), correlating with a much thicker overriding plate in the Nazca flat slab regions than in the Alaska case. Note that even with the many recent data collection efforts, which have greatly improved our understanding of the Yakutat plateau in Alaska, there is still much more to be learned about its time-dependent impact on the subducting plate geometry, including slab segmentation, as well as the time-dependent interplay between the downgoing and overriding plate structure.

9.5. CONCLUSIONS

This chapter provides broader geodynamics context for recent EarthScope seismic syntheses for Alaska and northwestern Canada based on data collected as a part of EarthScope. Specifically, key results from two recent EarthScope seismic syntheses are synthesized. In addition, a geodynamic modeling review is provided that focuses on continuum models of subduction, with applications to the Aleutian–Alaska subduction zone. The focused seismic studies are placed in the context of the vast geodynamics modeling literature with the goal of connecting the new constraints on the lithospheric and slab structure with insights on large-scale tectonic processes gained from generalized and regional subduction models. Avenues for future work are identified, including testing the effects of deeper slab structure on asthenospheric flow dynamics and upper plate deformation as well as time-dependent models of plateau/LIP subduction-collision on the subduction evolution in Alaska. Large-scale similarities and differences with other locations along the Pacific Ring of Fire are also identified. As data collection efforts continue to expand and modeling capabilities continue to improve, future comparative data analysis and modeling studies can continue to shed light on the dynamics of the Aleutian–Alaska subduction zone and in particular examine the region in the context of the Pacific Ring of Fire multi-plate tectonic system.

ACKNOWLEDGMENTS

This chapter grew out of discussions at the UNAVCO Alaska EarthScope and Beyond Virtual Seminar Series in Spring 2021 and the paired EarthScope Alaska and Beyond Virtual Workshop in May 2021, supported by the National Science Foundation and the National Aeronautics and Space Administration. M. Jadamec would like to thank Wesley K. Wallace, Magali Billen, Sarah Roeske, Louise Kellogg, and Donald Turcotte for many insightful discussions on Alaska tectonics over the course of her graduate career. In addition, M. Jadamec would like to acknowledge her NSF CAREER Award on subduction along the Pacific Ring of Fire. In addition, the authors sincerely thank conference organizers Jeffrey

Freymueller, Julie Elliot, Sarah Roeske, and Rick Aster, as well as participants at the meeting for thoughtful discussions. We are grateful to Carl Tape, two anonymous reviewers, and Jeffrey Freymueller for insightful comments that improved the manuscript. This work is supported by NSF CAREER Award NSF-EAR 1945513 awarded to M. Jadamec, startup funding at Purdue University to X. Yang, NSF-EAR 2042553 to S. S. Wei, NSF EAR-2053042808 and Woods Hole Oceanographic Institution OBS Instrument Center Postdoctoral Scholarship to M. E. Mann, and NSF EAR-1829401 to K. M. Fischer. Maps were made with GMT (Wessel et al., 2013, 2019).

AUTHOR CONTRIBUTIONS

M. Jadamec developed the geodynamics framework, wrote the initial draft, and created the Alaska tectonic setting/Pacific Ring of Fire maps, conceptual diagrams, and synthesis of viscous flow simulation results figures. G. Pavlis conducted and led the seismic synthesis vote map work on the slab and upper-mantle structure and made the vote map figure components, with the full results in Pavlis et al. (2024). X. Yang conducted the seismic domain analysis of the upper plate and made the figure components for the crust and lithosphere domain, with the full results in Yang et al. (2024). All authors contributed to the text through editing of the text and discussion of the synthesis data and geodynamic implications for Alaska. All authors were deeply involved in the progressive development of ideas described in the collaborative collection of chapters.

AVAILABILITY STATEMENT

No new data were generated for this review/geodynamics implications chapter. The sources for the tectonic setting data plotted in the maps in Figures 9.1 and 9.2 are included directly in the figure captions. Maps were plotted with GMT (Wessel et al., 2013). The data availability for the seismic synthesis compilation figures, Figure 9.3 and 9.4, are given in the Data Availability sections of Yang et al. (2024) and Pavlis et al. (2024), respectively.

REFERENCES

Abers, G. A., van Keken, P. E., Kneller, E. A., Ferris, A., & Stachnik, J. C. (2006). The thermal structure of subduction zones constrained by seismic imaging: Implications for slab dehydration and wedge flow. *Earth and Planetary Science Letters*, *241*, 387–397.

Alisic, L., Gurnis, M., Stadler, G., Burstedde, C., & Ghattas, O. (2012). Multi-scale dynamics and rheology of mantle flow with plates. *Journal of Geophysical Research: Solid Earth (1978–2012)*, *117*(B10).

Argus, D. F., Gordon, R. G., & DeMets, C. (2011). Geologically current motion of 56 plates relative to the no-net-rotation reference frame. *Geochemistry, Geophysics, Geosystems*, *12* (11).

Arrial, P.-A., & Billen, M. I. (2013). Influence of geometry and eclogitization on oceanic plateau subduction. *Earth and Planetary Science Letters*, *363*, 34–43.

Bauer, M. A., Pavlis, G. L., & Landes, M. (2014). Subduction geometry of the Yakutat terrane, southeastern Alaska. *Geosphere*, *10*(6), 1161–1176.

Benowitz, J., Layer, P., Armstrong, P., Perry, S., Haeussler, P., Fitzgerald, P., & VanLaningham, S. (2011). Spatial variations in focused exhumation along a continental-scale strike-slip fault: The Denali fault of the eastern Alaska Range. *Geosphere*, *7*(2), 455–467.

Benowitz, J. A., Roeske, S. M., Regan, S. P., Waldien, T. S., Elliott, J. L., & O'Sullivan, P. B. (2022, June). Large-scale, crustal-block vertical extrusion between the hines creek and Denali faults coeval with slip localization on the Denali fault since ca. 45 ma, hayes range, Alaska, USA. *Geosphere*, *18*, 1030–1054. Retrieved from https://doi.org/10.1130/GES02466.1. doi: 10.1130/GES02466.1

Berg, E. M., Lin, F. C., Allam, A., Schulte-Pelkum, V., Ward, K. M., & Shen, W. (2020). Shear velocity model of Alaska via joint inversion of Rayleigh wave ellipticity, phase velocities, and receiver functions across the Alaska transportable array. *Journal of Geophysical Research: Solid Earth*, *125*, e2019JB018582. doi: 10.1029/2019JB018582

Billen, M. I. (2008). Modeling the dynamics of subducting slabs. *Annual Reviews of Earth and Planetary Sciences*, *36*, 325–356.

Billen, M. I., & Gurnis, M. (2003). Comparison of dynamic flow models for the central Aleutian and Tonga-Kermadec subduction zones. *Geochemistry Geophysics Geosystems*, *4*(1035). doi: 10.1029/2001GC000295

Billen, M. I., Gurnis, M., & Simons, M. (2003). Multiscale dynamics of the Tonga-Kermadec subduction zone. *Geophysical Journal International*, *153*, 359–388.

Billen, M. I., & Hirth, G. (2004). Rheologic controls on the dynamic evolution of slabs in the upper mantle. *Eos Transactions AGU Fall Meeting Supplement*, *85*(47), T23D-03.

Billen, M. I., & Hirth, G. (2007). Rheological controls on slab dynamics. *Geochemistry Geophysics Geosystems*, *8*(Q08012). doi: 10.1029/2007GC001597

Bird, P. (1996). Computer simulations of Alaskan tectonics. *Tectonics*, *15*(2), 225–236.

Bird, P. (2003). An updated digital model of plate boundaries. *Geochemistry Geophysics Geosystems*, *4*(3), 1027. doi: 10.1029/2001GC000252

Bird, P., & Piper, K. (1980). Plane-stress finite-element models of tectonic flow in southern California. *Physics of the Earth and Planetary Interiors*, *21*(2–3), 158–175.

Boutelier, D., Chemenda, A., & Burg, J.-P. (2003). Subduction versus accretion of intra-oceanic volcanic arcs: Insight from thermo-mechanical analogue experiments. *Earth and Planetary Science Letters*, *212*(1), 31–45.

Brocher, T. M., Fuis, G. S., Fisher, M. A., Plafker, G., Taber, J. J., & Christensen, N. I. (1994). Mapping the megathrust beneath the northern Gulf of Alaska using wide-angle seismic data. *Journal of Geophysical Research*, *99*(B6), 11663–11685.

Brueseke, M. E., Benowitz, J. A., Bearden, A. T., Mann, M. E., & Miggins, D. P. (2023). Subduction disruption, slab tears: ca. 1 Ma true collision of an ∼30-km-thick oceanic plateau segment recorded by Yakutat slab nascent tear magmatism. *Terra Nova*, *35*(1), 49–57.

Brueseke, M. E., Benowitz, J. A., Trop, J. M., Davis, K. N., Berkelhammer, S. E., Layer, P. W., & Morter, B. K. (2019). The Alaska wrangell arc:∼30 ma of subduction-related magmatism along a still active arc-transform junction. *Terra Nova*, *31*(1), 59–66.

Bruns, T. (1983). Model for the origin of the Yakutat block, an accreting terrane in the northern Gulf of Alaska. *Geology*, *11*(12), 718.

Bryan, S. E., & Ferrari, L. (2013). Large igneous provinces and silicic large igneous provinces: Progress in our understanding over the last 25 years. *GSA Bulletin*, *125*(7–8), 1053–1078.

Burdick, S., Li, C., Martynov, V., Cox, T., Eakins, J., Mulder, T.,. et al. (2008). Upper mantle heterogeneity beneath North America from travel time tomogra-phy with global and USArray transportable array data. *Seismological Research Letters*, *79*(3), 384–392.

Burdick, S., Vernon, F.L., Martynov, V., Eakins, J., Cox, T., Tytell, J., et al. (2017). Model update may 2016: Upper-mantle heterogeneity beneath North America from travel-time tomography with global and USArray data. *Seismological Research Letters*, *88*(2A), 319–325.

Burkett, C. A., Bemis, S. P., & Benowitz, J. A. (2016). Along-fault migration of the Mount McKinley restraining bend of the Denali fault defined by late Quaternary fault patterns and seismicity, Denali National Park & Preserve, Alaska. *Tectonophysics*, *693*, 489–506.

Burkett, E. R., & Billen, M. I. (2009). Dynamics and implications of slab detachment due to ridge-trench collision. *Journal of Geophysical Research: Solid Earth (1978–2012)*, *114*(B12).

Burkett, E. R., & Billen, M. I. (2010). Three-dimensionality of slab detachment due to ridge-trench collision: Laterally simultaneous boudinage versus tear propagation. *Geochemistry, Geophysics, Geosystems*, *11*(11).

Christensen, D. H., & Abers, G. A. (2010). Seismic anisotropy under central Alaska from SKS splitting observations. *Journal of Geophysical Research*, *115*(B04315). doi: 10.1029/2009JB006712

Christensen, D. H., & Beck, S. L. (1994). The rupture process and tectonic implications of the great 1964 prince william sound earthquake. *Pure and applied geophysics*, *142*(1), 29–53.

Christeson, G., Gulick, S., van Avendonk, H., Worthington, L., Reece, R., & Pavlis, T. (2010). The Yakutat terrane: Dramatic change in crustal thickness across the Transition fault, Alaska. *Geology*, *38*(10), 895–898.

Cizkova, H., van Hunen, J., van den Berg, A. P., & Vlaar, N. J. (2002). The influence of rheological weakening and yield stress on the interaction of slabs with the 670 km discontinuity. *Earth and Planetary Science Letters*, *199*, 447–457.

Cloos, M. (1993). Lithospheric buoyancy and collisional orogenesis: Subduction of oceanic plateaus, continental margins, island arcs, spreading ridges, and seamounts. *Geological Society of America Bulletin*, *105*, 715–737.

Colpron, M., Nelson, J. L., & Murphy, D. C. (2007). Northern Cordilleran terranes and their interactions through time. *GSA today*, *17*(4), 4.

Conrad, C. P., & Lithgow-Bertelloni, C. (2006). Influence of continental roots and asthenosphere on plate-mantle coupling. *Geophysical Research Letters*, *33*(5), L05312.

Coulson, S., Garth, T., & Rietbrock, A. (2018). Velocity structure of the subducted Yakutat terrane, Alaska: Insights from guided waves. *Geophysical Research Let-ters*, *45*(8), 3420–3428.

Crameri, F., Schmeling, H., Golabek, G., Duretz, T., Orendt, R., Buiter, S., et al. (2012). A comparison of numerical surface topography calculations in geody-namic modelling: An evaluation of the 'sticky air' method. *Geophysical Journal International*, *189*(1), 38–54.

Crameri, F., Tackley, P., Meilick, I., Gerya, T. V., & Kaus, B. (2012). A free plate surface and weak oceanic crust produce single-sided subduction on Earth. *Geophysical Research Letters*, *39*(3), L03306.

Daly, K. A., Abers, G. A., Mann, M. E., Roecker, S., & Christensen, D. H. (2021). Subduction of an oceanic plateau across southcentral Alaska: High-resolution seismicity. *Journal of Geophysical Research: Solid Earth*, *126* (11), e2021JB022809.

DeMets, C., Gordon, R. G., & Argus, D. F. (2010). Geologically current plate mo-tions. *Geophysical journal international*, *181*(1), 1–80.

DeMets, C., Gordon, R. G., Argus, D. F., & Stein, S. (1994). Effect of recent revisions to the geomagnetic reversal time scale on estimates of current plate motions. *Geophysical Research Letters*, *218*(207–237), 2191–2194.

Eberhart-Phillips, D., Christensen, D. H., Brocher, T. M., Hansen, R., Ruppert, N. A., Haeussler, P. J., & Abers, G. A. (2006). Imaging the transition from Aleutian subduction to Yakutat collision in central Alaska, with local earthquakes and active source data. *Journal of Geophysical Research*, *111*(B11303). doi: 10.1029/2005JB004240

Eberhart-Phillips, D., Haeussler, P. J., Freymueller, J. T., Frankel, A. D., Rubin, C. M., Craw, P., et al. (2003). The 2002 Denali Fault Earthquake: A large magnitude, slip-partitioned event. *Science*, *300*, 1112–1118.

Elliott, J., & Freymueller, J. T. (2020). A block model of present-day kinematics of Alaska and western Canada. *Journal of Geophysical Research: Solid Earth*, *125*(7), e2019JB018378.

Elliott, J., Freymueller, J. T., & Larsen, C. F. (2013). Active tectonics of the St. Elias Orogen, Alaska, observed with gps measurements. *Journal of Geophysical Research: Solid Earth*, *118*(10), 5625–5642.

England, P., Houseman, G., & Sonder, L. (1985). Length scales for continental deformation in convergent, divergent, and strike-slip environments: Analytical and approximate solutions for a thin viscous sheet model. *Journal of Geophysical Research*, *90*, 3551–3557.

England, P., & McKenzie, D. (1982). A thin viscous sheet model for continental deformation. *Geophysical Journal of the Royal Astronomical Society*, *70*, 295–321.

Enkelmann, E., Zeitler, P., Garver, J., Pavlis, T., & Hooks, B. (2010). The thermochronological record of tectonic and surface process interaction at the Yakutat–North American collision zone in southeast Alaska. *American Journal of Science*, *310*(4), 231–260.

Enkelmann, E., Zeitler, P., Pavlis, T., Garver, J., & Ridgway, K. (2009). Intense localized rock uplift and erosion in the St. Elias orogen of Alaska. *Nature Geoscience*, *2*(5), 360–363.

Espurt, N., Funiciello, F., Martinod, J., Guillaume, B., Regard, V., Faccenna, C., & Brusset, S. (2008). Flat subduction dynamics and deformation of the South American plate: Insights from analog modeling. *Tectonics*, *27*(TC3011).

Estabrook, C. H., Nábělek, J. L., & Lerner-Lam, A. L. (1992). Tectonic model of the Pacific-North American Plate Boundary in the Gulf of Alaska from broadband analysis of the 1979 St. Elias, Alaska, earthquake and its aftershocks. *Journal of Geophysical Research: Solid Earth*, *97*(B5), 6587–6612.

Estève, C., Audet, P., Schaeffer, A. J., Schutt, D. L., Aster, R. C., & Cubley, J. F. (2020). Seismic evidence for craton chiseling and displacement of lithospheric mantle by the Tintina fault in the northern Canadian Cordillera. *Geology*, *48*(11), 1120–1125.

Estève, C., Schaeffer, A. J., & Audet, P. (2019). Upper mantle structure underlying the diamondiferous Slave Craton from teleseismic body-wave tomography. *Tectonophysics*, *757*, 187–202.

Faccenda, M., & Capitanio, F. (2012). Development of mantle seismic anisotropy during subduction-induced 3-d flow. *Geophysical Research Letters*, *39*(11).

Faccenna, C., & Becker, T. (2010). Shaping mobile belts by small-scale convection. *Nature*, *465*(7298), 602–605.

Feng, L., & Ritzwoller, M. H. (2019). A 3-d shear velocity model of the crust and uppermost mantle beneath Alaska including apparent radial anisotropy. *Journal of Geophysical Research: Solid Earth*, *124*, 10468–10497. doi: 10.1029/2019JB018122

Ferris, A., Abers, G. A., Christensen, D. H., & Veenstra, E. (2003). High resolution image of the subducted Pacific (?) plate beneath central Alaska, 50–150 km depth. *Earth and Planetary Science Letters*, *214*, 575–588.

Finzel, E. S., Flesch, L., & Ridgway, K. (2011). Kinematics of a diffuse North America–Pacific–Bering plate boundary in Alaska and western Canada. *Geology*, *39*(9), 835.

Finzel, E. S., Flesch, L. M., Ridgway, K. D., Holt, W. E., & Ghosh, A. (2015). Surface motions and intraplate continental deformation in Alaska driven by mantle flow. *Geophysical Research Letters*, *42*(11), 4350–4358.

Fischer, K. M., Parmentier, E. M., Stine, A. R., & Wolf, E. (2000). Modeling anisotropy and plate-driven flow in the Tonga subduction zone back arc. *Journal of Geophysical Research*, *105*(B7), 16181–16191.

Fisher, M. A., Nokleberg, W. J., Ratchkovski, N., Pellerin, L., Glen, J. M., Brocher, T. M., & Booker, J. (2004). Geophysical investigation of the Denali fault and Alaska Range orogen within the aftershock zone of the October-November 2002, M = 7.9 Denali fault earthquake. *Geology*, *32*, 269–272.

Fitzgerald, P. G., Roeske, S. M., Benowitz, J. A., Riccio, S. J., Perry, S. E., & Armstrong, P. A. (2014). Alternating asymmetric topography of the Alaska range along the strike-slip Denali fault: Strain partitioning and lithospheric control across a terrane suture zone. *Tectonics*, 33, 1519–1533, doi:10.1002/2013TC003432.

Fitzgerald, P. G., Stump, E., & Redfield, T. F. (1993). Late Cenozoic uplift and Denali and its relation to relative plate motion and fault morphology. *Science*, *259*, 497–499.

Flesch, L. M., Haines, A. J., & Holt, W. E. (2001). Dynamics of the India-Eurasia collision zone. *Journal of Geophysical Research*, *106*(B8), 435.

Fraters, M., Thieulot, C., Van Den Berg, A., & Spakman, W. (2019). The Geodynamic World Builder: A solution for complex initial conditions in numerical modeling. *Solid Earth*, *10*(5), 1785–1807.

Freymueller, J. T., Woodard, H., Cohen, S. C., Cross, R., Elliott, J., Larsen, C. F., et al. (2008). Active Tectonics and Seismic Potential of Alaska *Active tectonics and seismic potential of Alaska* (Vol. 179, p. 1–42). J. T. Freymueller, P. J. Haeussler, R. L. Wesson, & G. Ekström (Eds.). American Geophyscal Union.

Fuis, G. S., Ambos, E. L., Mooney, W. D., Christensen, N. I., & Geist, E. (1991). Crustal structure of accreted terranes in southern Alaska, Chugach Mountains and Copper River basin, from seismic refraction results. *Journal of Geophysical Research*, *96*, 4187–4227.

Fuis, G. S., Moore, T. E., Plafker, G., Brocher, T. M., Fisher, M. A., Mooney, W. D., et al. (2008). Trans-Alaska Crustal Transect and continental evolution involving subduction underplating and synchronous foreland thrusting. *Geology*, *36*, 267–270.

Funiciello, F., Faccenna, C., Giardini, D., & Regenauer-Lieb, K. (2003). Dynamics of retreating slabs: 2. Insights from three-dimensional laboratory experiments. *Journal of Geophysical Research*, *108*(B4), 2207. doi: 10.1029/2001JB000896

Funiciello, F., Faccenna, C., Heuret, A., Lallemand, S., Di Giuseppe, E., & Becker, T. (2008). Trench migration, net rotation and slab–mantle coupling. *Earth and Planetary Science Letters*, *271* (1–4), 233–240.

Funiciello, F., Moroni, M., Piromallo, C., Faccenna, C., Cenedese, A., & Bui, H. A. (2006). Mapping mantle flow during retreating subduction: Laboratory models analyzed by feature tracking. *Journal of Geophysical Research*, *111*(B03402). doi: 10.1029/2005JB003792

Fuston, S., & Wu, J. (2020). Raising the Resurrection Plate from an unfolded-slab plate tectonic reconstruction of northwestern North America since early Cenozoic time. *Geological Society of America Bulletin*, *133*(5–6), 1128–1140.

Gama, I., Fischer, K. M., Dalton, C.A., & Eilon, Z. (2022b, December). Variations in lithospheric thickness across the Denali fault and in northern Alaska. *Geophysical Research Letters*, e2022GL101256. doi: 10.1029/2022GL101256

Gama, I., Fischer, K. M., & Hua, J. (2022a, October). Mapping the lithosphere and asthenosphere beneath Alaska with Sp converted waves. *Geochemistry, Geophysics, Geosystems*, *23*, e2022GC010517. doi: 10.1029/2022GC010517

Garfunkel, Z., Anderson, C. A., & Schubert, G. (1986). Mantle circulation and the lateral migration of subducted slabs. *Journal of Geophysical Research*, *91*(B7), 7205–7223.

Gerya, T. V. (2011). Future directions in subduction modeling. *Journal of Geody namics*.

Gerya, T. V. (2022). Numerical modeling of subduction: State of the art and future directions. *Geosphere*, *18*(2), 503–561.

Gerya, T. V., Yuen, D. A., & Maresch, W. V. (2004). Thermomechanical modelling of slab detachment. *Earth and Planetary Science Letters*, *226*, 101–116.

Giuseppe, E. D., van Hunen, J., Funiciello, F., Faccenna, C., & Giardini, D. (2008). Slab stiffness control of trench motion: Insights from numerical models. *Geochemistry Geophysics Geosystems*, *9*(2), Q02014. doi: 10.1029/2007GC001776

Goes, S., Agrusta, R., van Hunen, J., & Garel, F. (2017). Subduction-transition zone interaction: A review. *Geosphere*, GES01476–1.

Gou, T., Zhao, D., Huang, Z., & Wang, L. (2019). Aseismic deep slab and mantle flow beneath Alaska: Insight from anisotropic tomography. *Journal of Geophysical Research: Solid Earth*, *124*(2), 1700–1724.

Govers, R., & Wortel, M. J. R. (2005). Lithosphere tearing at step faults: Response to edges of subduction zones. *Earth and Planetary Science Letters*, *236*, 505–523.

Gudmundsson, O., & Sambridge, M. (1998). A regionalized upper mantle (RUM) seismic model. *Journal of Geophysical Research*, *103*(B4), 7121–7136.

Gurnis, M., Turner, M., Zahirovic, S., DiCaprio, L., Spasojevic, S., Müller, R., et al. (2012). Plate tectonic reconstructions with continuously closing plates. *Computers & Geosciences*, *38*(1), 35–42.

Gutscher, M. A., Spakman, W., Bijwaard, H., & Engdahl, E. R. (2000). Geodynamics of flat subduction: Seismicity and tomographic constraints from the Andean margin. *Tectonics*, *19*(5), 814–833.

Haeussler, P. (2008). An overview of the neotectonics of interior Alaska: Farfield deformation from the Yakutat Microplate collision. In J. T. Freymueller, P. J. Haeussler, R. L. Wesson, & G. Ekström (Eds.), *Active tectonics and seismic potential of Alaska* (Vol. *179*, pp. 83–108). American Geophyscal Union.

Haeussler, P. J., Bradley, D. W., Wells, R. E., & Miller, M. L. (2003). Life and death of the Resurrection plate: Evidence for its existence and subduction in the northeastern Pacific in Paleocene-Eocene time. *GSA Bulletin*, *115* (7).

Hale, A. J., Gottschaldt, K.-D., Rosenbaum, G., Bourgouin, L., Bauchy, M., & Mühlhaus, H. (2010). Dynamics of slab tear faults: Insights from numerical modelling. *Tectonophysics*, *483* (1–2), 58–70.

Haney, M. M., Ward, K. M., Tsai, V. C., & Schmandt, B. (2020). Bulk structure of the crust and upper mantle beneath Alaska from an approximate rayleigh-wave dispersion formula. *Seismological Research Letters*, *91*, 3064–3075. doi: 10.1785/0220200162

Hanna, J., & Long, M. (2012). SKS splitting beneath Alaska: Regional variability and implications for subduction processes at a slab edge. *Tectonophysics*, 272–285.

Hayes, G., Moore, G. L., Portner, D. E., Hearne, M., Flamme, H., Furtney, M., & Smoczyk, G. M. (2018). Slab2, a comprehensive subduction zone geometry model. *Science*, *362*(6410), 58–61.

Haynie, K. L. (2019). *Controls of flat slab versus oceanic plateau subduction on overriding plate deformation in south-central Alaska*. PhD Dissertation. State University of New York at Buffalo.

Haynie, K. L., & Jadamec, M. A. (2017). Tectonic drivers of the Wrangell block: Insights on forearc sliver processes from 3D geodynamic models of Alaska. *Tectonics*, *36*, 28. doi: 10.1002/2016TC004410

Haynie, K. L., & Jadamec, M. A. (2024). Implications of variable plate coupling versus plateau buoyancy on subduction dynamics: A case study of the Yakutat plateau in Alaska. In N. A. Ruppert, M. A. Jadamec, & J. T. Freymueller (Eds.), *Tectonics and Seismicity of Alaska and Northwestern Canada: EarthScope and Beyond*. American Geophysical Union Wiley.

Holt, A., Becker, T., & Buffett, B. (2015). Trench migration and overriding plate stress in dynamic subduction models. *Geophysical Journal International*, *201*(1), 172–192.

Jadamec, M. A. (2016a). Insights on slab-driven mantle flow from advances in three-dimensional modelling. *Journal of Geodynamics*, *100*, 51–70. doi: dx.doi.org/10.1016/j.jog.2016.07.004

Jadamec, M. A. (2016b). Slab driven mantle weakening and rapid mantle flow. In G. Morra, D. A. Yuen, S.-M. Lee, & S. Stein (Eds.), *Subduction dynamics: From mantle flow to mega disasters* (Vol. *211*, chap. 7). Hoboken, NJ: John Wiley & Sons, Inc. doi: 10.1002/9781118888865

Jadamec, M. A., & Billen, M. I. (2010). Reconciling surface plate motions and rapid three-dimensional flow around a slab edge. *Nature*, *465*, 338–342.

Jadamec, M. A., & Billen, M. I. (2012). The role of rheology and slab shape on rapid mantle flow: Three-dimensional numerical models of the Alaska slab edge. *Journal of Geophysical Research*, *117*(B02304). doi: 10.1029/2011JB008563

Jadamec, M. A., Billen, M. I., & Kreylos, O. (2012). Three-dimensional simulations of geometrically complex subduction with large viscosity variations. In *Xsede '12 Proceedings of the 1st conference of the extreme science and engineering discovery environment: Bridging from the extreme to the campus and beyond* (pp. 1–8).

Jadamec, M. A., Billen, M. I., & Roeske, S. M. (2013). Three-dimensional numerical models of flat slab subduction and the Denali fault driving deformation in south-central Alaska. *Earth and Planetary Science Letters*, *376*, 29–42.

Jadamec, M. A., Kreylos, O., Chang, B., Fischer, K. M., & Yikilmaz, M. B. (2018a). Movies for: A visual survey of global slab geometries with ShowEarthModel and implications for a three-dimensional subduction paradigm. *Earth and Space Science (Digital Collection hosted at the University at Buffalo Institutional Repository (UBIR))*, Movie Downloads: http://hdl.handle.net/10477/76912. Movie Streams: http://goo.gl/Y7PDEX.

Jadamec, M. A., Kreylos, O., Chang, B., Fischer, K. M., & Yikilmaz, M. B. (2018b). A visual survey of global slab geometries with ShowEarthModel and implications for a three-dimensional subduction paradigm. *Earth and Space Science*, *5*, 18. doi: 10.1002/2017EA000349

Jarrard, R. D. (1986). Relations among subduction parameters. *Reviews of Geophysics*, *24*(2), 217–284.

Jiang, C., Schmandt, B., Ward, K. M., Lin, F., & Worthington, L. L. (2018). Upper mantle seismic structure of Alaska from Rayleigh and S wave tomography. *Geophysical Research Letters*, *45*, 10,350–10,359. doi: 10.1029/2018GL079406

Jordán, T. E., Isacks, B. L., Allmendinger, R. W., Brewer, J. A., Ramos, V. A., & Ando, C. J. (1983). Andean tectonics related to geometry of subducted Nazca plate. *Geological Society of America Bulletin*, *94*(3), 341–361.

Kalbas, J. L., Freed, A. M., & Ridgway, K. D. (2008). Contemporary fault mechanics in southern Alaska. *Geophysical Monograph Series*, *179*, 321–336.

Kaminiski, E., & Ribe, N. M. (2002). Timescales of the evolution of seismic anisotropy in mantle flow. *Geology, Geochemistry and Geophysics*, *3* (1). doi: 10.1029/2001GC000222

Karato, S., Jung, H., Katayama, I., & Skemer, P. (2008). Geodynamic significance of seismic anisotropy of the upper mantle: New insights from laboratory studies. *Annual Reviews of Earth and Planetary Sciences*, *36*, 59–95. doi: 10.1146/annurev.earth.36.031207.124120

Kim, Y., Abers, G. A., Li, J., Christensen, D., Calkins, J., & Rondenay, S. (2014). Alaska Megathrust 2: Imaging the megathrust zone and Yakutat/Pacific plate interface in the Alaska subduction zone. *Journal of Geophysical Research: Solid Earth*, *119*(3), 1924–1941.

Kincaid, C., & Griffiths, R. W. (2003). Laboratory models of the thermal evolution of the mantle during rollback subduction. *Nature*, *425*, 58–62.

King, S. D. (2001). Subduction zones: Observations and geodynamic models. *Physics of Earth and Planetary Interiors*, *127*, 9–24.

Kiraly, A., Portner, D., Haynie, K. L., Chilson-Parks, B. H., Ghosh, T., Jadamec, M. A., et al. (2020). The effect of slab gaps on subduction dynamics and mantle upwelling. *Tectonophysics*, *785* (228458). doi: doi.org/10.1016/j.tecto.2020.228458

Kneller, E. A., & van Keken, P. E. (2008). Effect of three-dimensional slab geometry on deformation in the mantle wedge: Implications for shear wave anisotropy. *Geochemistry Geophysics Geosystems*, *9* (Q01003). doi: 10.1029/2007GC001677

Koehler, R., Carver, G., & Commission, A. S. H. S. (2018). *Active faults and seismic hazards in Alaska* (Miscellaneous Publication No. 160). Alaska Division of Geological & Geophysical Surveys. doi: doi.org/10.14509/29705

Koons, P., Hooks, B., Pavlis, T., Upton, P., & Barker, A. (2010). Three-dimensional mechanics of Yakutat convergence in the southern Alaskan plate corner. *Tectonics*, *29*.

Kronbichler, M., Heister, T., & Bangerth, W. (2012). High accuracy mantle convection simulation through modern numerical methods. *Geophysical Journal International*, *191*(1), 12–29.

Lallemand, S., Heuret, A., & Boutelier, D. (2005). On the relationships between slab dip, back-arc stress, upper plate absolute motion, and crustal nature in subduction zones. *Geochemistry Geophysics Geosystems*, *6* (9), Q09006. doi: 10.1029/2005GC000917

Leo, J., Walker, A., Li, Z.-H., Wookey, J., Ribe, N., Kendall, J.-M., & Tommasi, A. (2014). Development of texture and seismic anisotropy during the onset of subduction. *Geochemistry, Geophysics, Geosystems*.

Li, J., Abers, G. A., Kim, Y., & Christensen, D. (2013). Alaska megathrust 1: Seismicity 43 years after the great 1964 Alaska Megathrust Earthquake. *Journal of Geophysical Research: Solid Earth*, *118*(9), 4861–4871.

Li, Z.-H., Di Leo, J. F., & Ribe, N. M. (2014). Subduction-induced mantle flow, finite strain and seismic anisotropy: Numerical modeling. *Journal of Geophysical Research: Solid Earth*.

Liu, L., & Stegman, D. (2012). Origin of Columbia River flood basalt controlled by propagating rupture of the Farallon slab. *Nature*, *482*(7385), 386–389.

Liu, S., & Currie, C. A. (2016). Farallon plate dynamics prior to the Laramide orogeny: Numerical models of flat subduction. *Tectonophysics*, *666*, 33–47.

Liu, X., & Currie, C. A. (2019). Influence of upper plate structure on flat-slab depth: Numerical modeling of subduction dynamics. *Journal of Geophysical Research: Solid Earth*, *124*(12), 13150–13167.

Long, M., & Wirth, E. A. (2013). Mantle flow in subduction systems: The mantle wedge flow field and implications for wedge processes. *Journal of Geophysical Research*. doi: 10.1002/jgrb.50063

Long, M. D. (2013). Constraints on subduction geodynamics from seismic anisotropy. *Reviews of Geophysics*, *51*(1), 76–112.

Long, M. D., & Becker, T. W. (2010). Mantle dynamics and seismic anisotropy. *Earth and Planetary Science Letters*, *297*(3), 341–354.

Long, M. D., & Silver, P. G. (2008). The subduction zone flow field from seismic anisotropy: A global view. *Science*, *319*, 315–318.

Lonsdale, P. (1988). Paleogene history of the Kula plate: Offshore evidence and onshore implications. *Geological Society of America Bulletin*, *100* (5), 733.

Lundgren, P., Saucier, F., Palmer, R., & Langon, M. (1995). Alaska crustal deformation: Finite element modeling constrained by geologic and very long baseline interferometry data. *Journal of Geophysical Research*, *100*(B11), 22033–22045.

MacDougall, J. G., Jadamec, M. A., & Fischer, K. M. (2017). The zone of influence of the subducting slab in the asthenospheric mantle. *Journal of Geophysical Research*, 26 p. Retrieved from http://dx.doi.org/10.1002/2017JB014445 doi: 10.1002/2017JB014445

MacDougall, J. G., Kincaid, C., Szwaja, S., & Fischer, K. M. (2014). The impact of slab dip variations, gaps, and rollback on mantle wedge flow: Insights from fluids experiments. *Geophysical Journal International*, doi: 10.1093/gji/ggu053

Madsen, J. K., Thorkelson, D. J., Friedman, R. M., & Marshall, D. D. (2006). Cenozoic to recent plate configurations in the Pacific basin: Ridge subduction and slab window magmatism in western North America. *Geosphere*, *2*(1), 11–34.

Magni, V., Faccenna, C., van Hunen, J., & Funiciello, F. (2014). How collision triggers backarc extension: Insight into Mediterranean style of extension from 3-D numerical models. *Geology*, *42*(6), 511–514.

Manea, V. C., Pérez-Gussinyé, M., & Manea, M. (2012). Chilean flat slab subduction controlled by overriding plate thickness and trench rollback. *Geology*, *40*(1), 35–38.

Mann, M. E., Abers, G. A., Daly, K. A., & Christensen, D. H. (2022). Subduction of an oceanic plateau across southcentral Alaska: Scattered-wave imaging. *Journal of Geophysical Research: Solid Earth*, *127* (1), e2021JB022697.

Martinod, J., Funiciello, F., Faccenna, C., Labanieh, S., & Regard, V. (2005). Dynamical effects of subducting ridges: Insights from 3D laboratory models. *Geophysical Journal International*, *163*, 1137–1150.

Martinod, J., Guillaume, B., Espurt, N., Faccenna, C., Funiciello, F., & Regard, V. (2013). Effect of aseismic ridge subduction on slab geometry and overriding plate deformation: Insights from analogue modeling. *Tectonophysics*, *588*, 39–55.

Martin-Short, R., Allen, R., Bastow, I. D., Porritt, R. W., & Miller, M. S. (2018). Seismic imaging of the Alaska subduction zone: Implications for slab geometry and volcanism. *Geochemistry, Geophysics, Geosystems*, *19*, 4541–4560. doi: 10.1029/2018GC007962

Mason, W. G., Moresi, L. N., Betts, P. G., & Miller, M. S. (2010). Three-dimensional numerical models of the influence of a buoyant oceanic plateau on subduction zones. *Tectonophysics*, *483*, 71–79.

Mazzotti, S., & Hyndman, R.D. (2002). Yakutat collision and strain transfer across the northern Cordillera. *Geology*, *30*(6), 495–498.

McConeghy, J., Flesch, L., & Elliott, J. (2022). Investigating the effect of mantle flow and viscosity structure on surface velocities in Alaska using 3-D geodynamic models. *Journal of Geophysical Research: Solid Earth*, *127*. doi: 10.1029/2022JB024704

McPherson, A., Christensen, D., Abers, G., & Tape, C. (2020). Shear wave splitting and mantle flow beneath Alaska. *Journal of Geophysical Research: Solid Earth*, *125* (4), e2019JB018329.

Miller, M. S., & Moresi, L. N. (2018). Mapping the Alaskan moho. *Seismological Research Letters*, *89*(6), 2430–2436.

Miller, M. S., Ruppert, N. A., & Abers, G. (2020). Introduction to the focus section on EarthScope Alaska and Canada. *Seismological Society of America*, *91*(6), 3015–3016.

Millet, F., Rondenay, S., Bodin, T., & Tape, C. (2023). Seismic imaging of the west-ward transition from Yakutat to Pacific subduction in southern Alaska. *Geochemistry, Geophysics, Geosystems*, *24* (11), e2022GC010374.

Moore, T. E., & Box, S. E. (2016). Age, distribution and style of deformation in Alaska north of 60 N: Implications for assembly of Alaska. *Tectonophysics*, *691*, 133–170.

Moresi, L. N., Betts, P., Miller, M., & Cayley, R. (2014). Dynamics of continental accretion. *Nature*, *508*(7495), 245–248.

Moresi, L. N., & Gurnis, M. (1996). Constraints on the lateral strength of slabs form three-dimensional dynamic flow models. *Earth and Planetary Science Letters*, *138*, 15–28.

Moresi, L. N., & Solomatov, V. S. (1995). Numerical investigation of 2D convection with extremely large viscosity variations. *Physics of Fluids*, *7*(9), 2154–2162.

Morra, G., Regenauer-Lieb, K., & Giardini, D. (2006). Curvature of oceanic arcs. *Geology*, *34*(10), 877–880.

Müller, R. D., Cannon, J., Qin, X., Watson, R. J., Gurnis, M., Williams, S., et al. (2018). Gplates: building a virtual earth through deep time. *Geochemistry, Geophysics, Geosystems*, *19*(7), 2243–2261.

Müller, R. D., Zahirovic, S., Williams, S. E., Cannon, J., Seton, M., Bower, D. J. et al. (2019). A global plate model including lithospheric deformation along major rifts and orogens since the Triassic. *Tectonics*, *38*(6), 1884–1907.

Nayak, A., Eberhart-Phillips, D., Ruppert, N. A., Fang, H., Moore, M. M., Tape, C., et al. (2020). 3D seismic velocity models for Alaska from joint tomographic inversion of body-wave and surface-wave data. *Seismological Research Letters*, *91*, 3106–3119. doi: 10.1785/0220200214

Nokleberg, W. J., MollStalcup, E., Miller, T., Brew, D., Grantz, A., Reed Jr, J., et al. (1994). *Tectonostratigraphic terrane and overlap assemblage map of Alaska*. US Geological Survey, Open-File Report 94–194.

Nokleberg, W. J., Plafker, G., & Wilson, F. H. (1994). Geology of south-central Alaska. In G. Plafker & H. Berg (Eds.), *The Geology of North America* (Vols. G1, The Geology of Alaska, pp. 311–366). Boulder, CO: Geological Society of America.

Paczkowski, K., Thissen, C. J., Long, M. D., & Montési, L. G. (2014). Deflection of mantle flow beneath subducting slabs and the origin of subslab anisotropy. *Geophysical Research Letters*, *41*(19), 6734–6742.

Page, R. A., Stephens, C. D., & Lahr, J. C. (1989). Seismicity of the Wrangell and Aleutian Wadati-Benioff zones and the North American plate along the Trans-Alaska Crustal Transect, Chugach Mountains and Copper River Basin, southern Alaska. *Journal of Geophysical Research*, *94*(B11), 16059–16082.

Pavlis, G. L., Bauer, M. A., Elliott, J. L., Koons, P., Pavlis, T. L., Ruppert, N., et al. (2019). A unified three-dimensional model of the lithospheric structure at the subduction corner in southeast Alaska: Summary results from STEEP. *Geosphere*, *15*, 382–406. doi: 10.1130/GES01488.1

Pavlis, G. L., Jadamec, M. A., Mann, M. E., Yang, X., Schaeffer, A., Wei, S. S., & Fischer, K. M. (2024). Synthesis of the seismic structure of the greater Alaska Region: Subducting slab geometry. In N. A. Ruppert, J. T. Freymueller, & M. A. Jadamec (Eds.), *Tectonics of Alaska and Northwestern Canada: EarthScope and Beyond*. American Geophysical Union Wiley.

Perttu, A., Christensen, D., Abers, G., & Song, X. (2014). Insights into mantle structure and flow beneath Alaska based on a decade of observations of shear wave splitting. *Journal of Geophysical Research: Solid Earth*, *119*(11), 8366–8377.

Piromallo, C., Becker, T. W., Funiciello, F., & Faccenna, C. (2006). Three-dimensional instantaneous mantle flow induced by subduction. *Geophysical Research Letters*, *33*, L08304.

Plafker, G., & Berg, H. (1994). *Overview of the geology and tectonic evolution of Alaska* (Vol. G1, pp. 989–1021). G. Plafker & H. Berg (Eds.). Geological Society of America.

Plafker, G., Gilpin, L. M., & Lahr, J. C. (1994). Plate 12: Neotectonic Map of Alaska. In G. Plafker & H. Berg (Eds.), *The Geology of North America* (Vols. G1, The Geology of Alaska). Boulder, CO: Geological Society of America.

Plafker, G., Moore, J. C., & Winkler, G. R. (1994). Geology of the southern Alaska margin. In G. Plafker & H. Berg (Eds.), *The Geology of North America* (Vols. G1, The Geology of Alaska, pp. 389–449). Boulder, CO: Geological Society of America.

Preece, S. J., & Hart, W. K. (2004). Geochemical variations in the <5 Ma Wrangell volcanic field, Alaska: Implications for the magmatic and tectonic development of a complex continental arc system. *Tectonophysics*, *392*, 165–191.

Qi, C., Zhao, D., & Chen, Y. (2007). Search for deep slab segments under Alaska. *Physics of the Earth and Planetary Interiors*, *165*, 68–82.

Rabade, S., Lin, F.-C., Tape, C., Ward, K. M., Waldien, T., & Allam, A. (2023). The crustal magmatic structure beneath the Denali Volcanic Gap imaged by a dense linear seismic array. *Journal of Geophysical Research: Solid Earth*, *128* (12), e2023JB027152.

Ratchkovski, N. A., & Hansen, R. A. (2002a). New constraints on tectonics of interior Alaska: Earthquake locations, source mechanism, and stress regime. *Bulletin of the Seismological Society of America*, *92*, 998–1014.

Ratchkovski, N. A., & Hansen, R. A. (2002b). New evidence for segmentation of the Alaska subduction zone. *Bulletin of the Seismological Society of America*, *92*(5), 1754–1765.

Ratchkovski, N. A., Wiemer, S., & Hansen, R. A. (2004). Seismotectonics of the central Denali fault, Alaska, and the 2002 Denali fault earthquake sequence. *Bulletin of the Seismological Society of America*, *94*(6B), S156–S174.

Redfield, T. F., Scholl, D. W., Fitzgerald, P. G., & M. E. Beck, J. (2007). Escape tectonics and the extrusion of Alaska: Past, present, and future. *Geology*, *35*(11), 1039–1042.

Ribe, N. M. (2007). Analytical approaches to mantle dynamics. *Mantle Dynamics*, *7*, 167–226.

Richards, C., Tape, C., Abers, G. A., & Ross, Z. E. (2021). Anisotropy variations in the Alaska subduction zone based on shear-wave splitting from intraslab earthquakes. *Geochemistry, Geophysics, Geosystems*, *22* (5), e2020GC009558.

Rodríguez-González, J., Negredo, A. M., & Billen, M. I. (2012). The role of the overriding plate thermal state on slab dip variability and on the occurrence of flat subduction. *Geochemistry, Geophysics, Geosystems*, *13* (1).

Rondenay, S., Montesi, L. G. J., & Abers, G. A. (2010). New geophysical insight into the origin of the Denali volcanic gap. *Geophysical Journal International*, *182*, 613–630.

Rossi, G., Abers, G. A., Rondenay, S., & Christensen, D. H. (2006). Unusual mantle Poisson's ratio, subduction, and crustal structure in central Alaska. *Journal of Geophysical Research*, *111* (B09311).

Royden, L. H., & Husson, L. (2006). Trench motion, slab geometry and viscous stresses in subduction systems. *Geophysical Journal International*, *167*(2), 881–905.

Rudi, J., Malossi, A. C. I., Isaac, T., Stadler, G., Gurnis, M., Staar, P. W., et al. (2015). An extreme-scale implicit solver for complex PDEs: highly heterogeneous flow in earth's mantle. In *Proceedings of the international conference for high performance computing, networking, storage and analysis* (pp. 1–12).

Savage, M. K. (1999). Seismic anisotropy and mantle deformation: What have we learned from shear wave splitting? *Reviews of Geophysics*, *374*(12), 65–106.

Schellart, W. P. (2004). Kinematics of subduction and subduction-induced flow in the upper mantle. *Journal of Geophysical Research*, *109* (B07401). doi: 10.1029/2004JB002970

Schellart, W. P. (2005). Influence of the subducting plate velocity on the geometry of the slab and migration of the subduction hinge. *Earth and Planetary Sci-ence Letters*, *231*, 197–219.

Schellart, W. P. (2008). Overriding plate shortening and extension above subduction zones: A parametric study to explain formation of the Andes Mountains. *Geological Society of America Bulletin*, *120*(11/12), 1441–1454.

Schellart, W. P. (2010a). Evolution of subduction zone curvature and its dependence on the trench velocity and the slab to upper mantle viscosity ratio. *Journal of Geophysical Research*, *115* (B11406). doi: 10.1029/2009JB006643

Schellart, W. P. (2010b). Mount Etna-Iblean volcanism caused by rollback-induced upper mantle upwelling around the Ionian slab edge: An alternative to the plume model. *Geology*, *38*(8), 691–694.

Schellart, W. P. (2023). Subduction zones: A short review. *Dynamics of Plate Tectonics and Mantle Convection*, 321–355.

Schellart, W. P., Freeman, J., Stegman, D. R., Moresi, L. N., & May, D. (2007). Evolution and diversity of subduction zones controlled by slab width. *Nature*, *446*, 308–311. doi: 10.1038

Schellart, W. P., Stegman, D. R., & Freeman, J. (2008). Global trench migration velocities and slab migration induced upper mantle volume fluxes: Constraints to find an Earth reference frame based on minimizing viscous dissipation. *Earth Science Reviews*, *88*, 118–144.

Schellart, W. P., & Strak, V. (2016). A review of analogue modelling of geodynamic processes: Approaches, scaling, materials and quantification, with an application to subduction experiments. *Journal of Geodynamics*, *100*, 7–32.

Schultz, R. A., & Aydin, A. (1990). Formation of interior basins associated with curved faults in Alaska. *Tectonics*, *9*(6), 1387–1407.

Sdrolias, M., & Müller, R. D. (2006). Controls on back-arc basin formation. *Geochemistry Geophysics Geosystems*, *7*(4), Q04016. doi: 10.1029/2005GC001090

Sébrier, M., Mercier, J. L., Macharé, J., Bonnot, D., Cabrera, J., & Blanc, J. L. (1988). The state of stress in an overriding plate situated above a flat slab: The Andes of central Peru. *Tectonics*, *7*(4), 895–928.

Seton, M., Müller, R. D., Zahirovic, S., Williams, S., Wright, N. M., Cannon, J., et al. (2020). A global data set of present-day oceanic crustal age and seafloor spreading parameters. *Geochemistry, Geophysics, Geosystems*, *21* (10), e2020GC009214.

Sharples, W., Jadamec, M. A., Moresi, L. N., & Capitanio, F. (2014). Overriding plate controls on subduction evolution. *Journal of Geophysical Research*, *119*, 6684–6704. doi: 10.1002/2014JB011163

Shephard, G. E., Matthews, K. J., Hosseini, K., & Domeier, M. (2017). On the consistency of tomographically imaged lower mantle slabs. *Geophysical Research Abstracts*, *19*, @Abstract EGU2017 -7916.

Skulski, T., Francis, D., & Ludden, J. (1991). Arc-transform magmatism in the Wrangell volcanic belt. *Geology*, *19*, 11–14.

Smithsonian. (2012). *Smithsonian institution, global volcanism program*. Retrieved from http://www.volcano.si.edu/world/globallists.cfm

Sobolev, S., & Babeyko, A. (2005). What drives orogeny in the Andes? *Geology*, *33*(8), 617.

Stadler, G., Gurnis, M., Burstedde, C., Wilcox, L. C., Alisic, L., & Ghattas, O. (2010). The dynamics of plate tectonics and mantle flow: From local to global scales. *Science*, *329*, 1033–1038.

Stegman, D. R., Farrington, R., Capitanio, F. A., & Schellart, W. P. (2010). A regime diagram for subduction styles from

3-D numerical models of free subduction. *Tectonophysics*, *483*(1–2), 29–45.

Stegman, D. R., Freeman, J., Schellart, W. P., Moresi, L. N., & May, D. (2006). Influence of trench width on subduction hinge retreat rates in 3D models of slab rollback. *Geochemistry Geophysics Geosystems*, *7*(3), Q03012. doi: 10.1029/2005GC001056

Stephens, C. D., Fogleman, K. A., Lahr, J. C., & Page, R. A. (1984). Wrangell Benioff zone, southern Alaska. *Geology*, *12*, 373–376.

Stern, R. J., & Gerya, T. (2018). Subduction initiation in nature and models: A review. *Tectonophysics*, *746*, 173–198.

Strak, V., & Schellart, W. P. (2014). Evolution of 3-D subduction-induced mantle flow around lateral slab edges in analogue models of free subduction analysed by stereoscopic particle image velocimetry technique. *Earth and Planetary Science Letters*, *403*, 368–379.

Suleimani, E., & Freymueller, J. T. (2020). Near-field modeling of the 1964 Alaska tsunami: The role of splay faults and horizontal displacements. *Journal of Geophysical Research: Solid Earth*, *125*(7), e2020JB019620.

Syracuse, E. M., & Abers, G. A. (2006). Global compilation of variations in slab depth beneath arc volcanoes and implications. *Geochemistry Geophysics Geosystems*, *7*(5), Q05017. doi: 10.1029/2005GC001045

Syracuse, E. M., van Keken, P., & Abers, G. (2010). The global range of subduction zone thermal models. *Physics of the Earth and Planetary Interiors*, *183*(1), 73–90.

Torne, M., Jimenez-Munt, I., Verges, J., Fernandez, M., Carballo, A., & Jadamec, M. A. (2019). Regional crustal and lithospheric thickness model for Alaska, the Chukchi Shelf, and the inner and outer Bering Shelves. *Geophysical Journal International*, *ggz424*. doi: https://doi.org/10.1093/gji/ggz424

Tovish, A., & Schubert, G. (1978). Island arc curvature, velocity of convergence and angle of subduction. *Geophysical Research Letters*, *5*(5), 329–332.

Tozer, B., Sandwell, D. T., Smith, W. H., Olson, C., Beale, J., & Wessel, P. (2019). Global bathymetry and topography at 15 arc sec: SRTM15+. *Earth and Space Science*, *6*(10), 1847–1864.

Turcotte, D. L., & Schubert, G. (2014). *Geodynamics* (3rd ed.). Cambridge University Press.

van Hunen, J., Van Den BERG, A. P., & Vlaar, N. J. (2002). On the role of subducting oceanic plateaus in the development of shallow flat subduction. *Tectonophysics*, *352*(3), 317–333.

van Hunen, J., van den Berg, A. P., & Vlaar, N. J. (2004). Various mechanisms to induce present-day shallow flat subduction and implications for the younger Earth: A numerical parameter study. *Physics of the Earth and Planetary Interiors*, *146*(1), 179–194.

van Keken, P. E., Currie, C., King, S. D., Behn, M. D., Cagnioncle, A., He, J., et al. (2008). A community benchmark for subduction zone modeling. *Physics of the Earth and Planetary Interiors*, *171*(1), 187–197.

Van Zelst, I., Crameri, F., Pusok, A. E., Glerum, A., Dannberg, J., & Thieulot, C. (2022). 101 geodynamic modelling: How to design, interpret, and communicate numerical studies of the solid Earth. *Solid Earth*, *13*(3).

Veenstra, E., Christensen, D. H., Abers, G. A., & Ferris, A. (2006). Crustal thickness variation in south-central Alaska. *Geology*, *34*(9), 781–784.

Veilleux, A. M., & Doser, D. I. (2007). Studies of Wadati-Benioff Zone seismicity of the Anchorage, Alaska, region. *Bulletin of the Seismological Society of America*, *97*(1B), 52–62.

Venereau, C., Martin-Short, R., Bastow, I. D., Allen, R. M., & Kounoudis, R. (2019). The role of variable slab dip in driving mantle flow at the eastern edge of the Alaskan subduction margin: Insights from shear-wave splitting. *Geochemistry, Geophysics, Geosystems*, *20*(5), 2433–2448.

Vogt, K., & Gerya, T. V. (2014). From oceanic plateaus to allochthonous terranes: Numerical modelling. *Gondwana Research*, *25* (2), 494–508.

Wada, I., He, J., Hasegawa, A., & Nakajima, J. (2015). Mantle wedge flow pattern and thermal structure in Northeast Japan: Effects of oblique subduction and 3-D slab geometry. *Earth and Planetary Science Letters*, *426*, 76–88.

Wallace, W., & Engebretson, D. (1984). Relationships between plate motions and Late Cretaceous to Paleogene magmatism in southwestern Alaska. *Tectonics*, *3*(2), 295–315.

Wallace, W. K. (2008). Yakataga fold-and-thrust belt: Structural geometry and tectonic implications of a small continental collision zone. *Active tectonics and seismic potential of Alaska* (pp. 237–256).

Wang, Y., & Tape, C. (2014). Seismic velocity structure and anisotropy of the Alaska subduction zone based on surface wave tomography. *Journal of Geophysical Research: Solid Earth*.

Ward, K. M., & Lin, F. C. (2018). Lithospheric structure across the Alaskan cordillera from the joint inversion of surface waves and receiver functions. *Journal of Geophysical Research: Solid Earth*, *123*, 8780–8797. doi: 10.1029/2018JB015967

Wessel, P., Luis, J., Uieda, L., Scharroo, R., Wobbe, F., Smith, W. H., & Tian, D. (2019). The generic mapping tools version 6. *Geochemistry, Geophysics, Geosystems*, *20* (11), 5556–5564.

Wessel, P., Smith, W. H., Scharroo, R., Luis, J., & Wobbe, F. (2013). Generic mapping tools: Improved version released. *Eos, Transactions American Geophysical Union*, *94* (45), 409–410.

Williams, M. L., Fischer, K. M., Freymueller, J. T., Tikoff, B., Tréhu, A. M., Aster, R., et al. (2010, February). *Unlocking the secrets of the North American continent: An EarthScope Science Plan for 2010–2020*. EarthScope, 78 pp.

Worthington, L. L., Van Avendonk, H. J., Gulick, S. P., Christeson, G. L., & Pavlis, T. L. (2012). Crustal structure of the Yakutat terrane and the evolution of subduction and collision in southern Alaska. *Journal of Geophysical Research: Solid Earth (1978–2012)*, *117* (B1).

Yang, X., & Gao, H. (2020). Segmentation of the Aleutian–Alaska subduction zone revealed by full-wave ambient noise tomography: Implications for the along-strike variation of volcanism. *Journal of Geophysical Research: Solid Earth*, *125* (11), e2020JB019677.

Yang, X., Mann, M. E., Fischer, K. M., Jadamec, M. A., Wei, S. S., Pavlis, G., & Schaeffer, A. (2024). Synthesis of the seismic structure of the greater Alaska region: Continental lithosphere. In N. A. Ruppert, J. T. Freymueller, & M. A. Jadamec

(Eds.), *Tectonics of Alaska and Northwestern Canada: EarthScope and Beyond*. American Geophysical Union Wiley.

Zhang, Y., Li, A., & Hu, H. (2019). Crustal structure in Alaska from receiver function analysis. *Geophysical Research Letters*, *46*, 1284–1292. doi: 10.1029/2018GL081011

Zhao, D., Christensen, D., & Pulpan, H. (1995). Tomographic imaging of the Alaska subduction zone. *Journal of Geophysical Research*, *100*(B4), 6487–6504.

Zhong, S. (2006). Constraints on thermochemical convection of the mantle from plume heat flux, plume excess temperature, and upper mantle temperature. *Journal of Geophysical Research*, *111*(B04409). doi: 10.1029/2005JB003972

Zhong, S., Yuen, D., Moresi, L. N., & Knepley, M. (2015). Numerical methods for mantle convection. In G. Schubert (Ed.), *Treatise on geophysics* (2nd ed., Vol. *7*). Elsevier.

Zhong, S., Zuber, M. T., Moresi, L. N., & Gurnis, M. (2000). Role of temperaturedependent viscosity and surface plates in spherical shell models of mantle convection. *Journal of Geophysical Research*, *105*(B5), 11063–11082.

Zweck, C., Freymueller, J. T., & Cohen, S. C. (2002). Three-dimensional elastic dislocation modeling of the postseismic response to the 1964 Alaska earthquake. *Journal of Geophysical Research*, *107*(B4), 2001JB000409.